https://doi.org/10.5194/egusphere-2025-2777
Preprint. Discussion started: 10 July 2025

Traffic impact modeling in SURFEX-TEB V9.0 model for improved road surface temperature prediction

Gabriel Colas[1], Valéry Masson[1], François Bouttier[1], and Ludovic Bouilloud[2]

[1]CNRM, Université de Toulouse,Météo-France, CNRS, Toulouse, France
[2]Météo-France, Toulouse, France

Correspondence: Gabriel Colas (gabriel.colas@meteo.fr)

Abstract. The impact of road traffic on local climate has often been overlooked, being modelled as an aggregated sensible heat flux released into the atmosphere, although it has multiple effects including turbulence, heat from energy inefficiencies of vehicles, tyre friction, snow compaction, and shadowing. These effects can impact the road surface conditions and exacerbate the phenomenon of Urban Heat Island (UHI). This study aims to improve the representation of traffic impacts in the Town Energy Balance (TEB) V9.0 urban climate model. Particular attention has been paid to preserve physical consistency among the parameterisations of tyre friction, turbulence, energy inefficiencies, and radiation impacts of the road traffic within the model. In addition, a method has been developed to model the average engine efficiency of the entire automobile fleet with internal combustion engines (ICEs) using the Worldwide Harmonized Light vehicles Test Cycles (WLTC). The new parameterisations are evaluated using observations from two road weather stations in southern Finland, Nupuri and Palojärvi, which are characterised by clear commuting patterns. To evaluate the new traffic parameterisation, road surface temperature (RST) differences between the two road carriageways is used to isolate the traffic-induced effects from natural factors. The results show that the new parameterisation is able to simulate the traffic-induced impacts on road surface temperatures. In addition, wind-induced impact and rolling friction have been shown to drive traffic effects on RST. Taking explicitly into account the traffic impacts might be better suited to simulate their actual impacts on the local scale.

1 Introduction

Road traffic has increased from 4.5 trillion passenger kilometres travelled in 1995 to 6 trillion in 2019, and from 2.4 billion tonne-km travelled for freight in 1995 to 3.3 billion in European Union in 2019 (EEA, 2024). The transport sector is a massive source of greenhouse gases, with the land transport sector being the fourth largest contributor, with long-term effects on global climate (IPCC, 2022). In addition to the long-term impacts on global climate, the cumulative effects of local dense road traffic significantly influence local climate and air quality. Road traffic is an important source of heat, pollution, turbulence, friction with the surface, and it impacts the local energy balance. Cities that concentrate both a large population and high traffic are

https://doi.org/10.5194/egusphere-2025-2777
Preprint. Discussion started: 10 July 2025

particularly impacted. At rush hour, some road segments on the Paris ring road can reach up to 220 0000 vehicles a day (Amato et al., 2016). No studies have attempted to assess or simulate the complete set of traffic impacts on local climate, which reveals a gap in existing weather and climate modelling tools.

A significant amount of the primary energy source of the motor vehicle transformed into mechanical power is lost and released as sensible and latent heat in the atmosphere. For vehicles equipped with internal combustion engines, that is, approximately 98% of the total automobile fleet in Europe in 2023 (Eurostat, 2023), more than 75% of the fuel combustion energy is lost (Johnson and Joshi, 2018). It is released as heat in the urban canopy along with house heating, air conditioning systems (de Munck et al., 2013) and energy loss from industries. In cities, traffic can be an important contributor to the total anthropogenic heat released in the air. The relative contribution of traffic to anthropogenic heat is greater in summer than in winter (Bohnenstengel et al., 2013; Pigeon et al., 2007). However, the impact of traffic on the local climate is greater in winter, particularly at rush hours (Pigeon et al., 2007; Iamarino et al., 2011). Many methods are available to estimate the heat released from the building sector (Bueno et al., 2012; Iamarino et al., 2011; Best and Grimmond,2016). On the contrary, there are few methods for the heat released by traffic. It can be modelled as an estimate aggregated with the other sources of anthropogenic heat (Varquez et al.,2021; Flanner,2009) or modelled separately (Pigeon et al.,2007; Ward et al., 2022; Sailor and Lu,2004). Modelled separately, the heat released by traffic is estimated mainly from inventories approach, with the average fuel consumption over the entire transport sector (Kłysik, 1996), or from vehicle fuel consumption statistics (Iamarino et al.,2011; Harrison et al.,1984; Pigeon et al.,2007) or from arbritray estimates (Sailor and Lu, 2004). Most of the other impacts of traffic, such as turbulence, friction with the surface, and changes in local energy balance, are not taken into account.

A moving vehicle has direct effects on the surface energy balance as well as on local turbulence. The tyres oppose a rolling resistance to the direction due to their viscoelastic properties, leading to thermomechanical impacts. Tyres warm up mainly due to the hysteresis effect (Lin and Hwang, 2004) and road warms up through friction and conduction (Kelly and Sharp, 2012; Logan, 2012). Thus, traffic can lead to increased road surface temperature (Fujimoto et al., 2008; Khalifa et al., 2016), snow compaction (Wahlin et al., 2014), and water splashing (Karsisto, 2024; Denby et al., 2013). In addition, a vehicle body is a moving obstacle immersed in the air with drag amount based on the structure of the flow in its wake (Ahmed, 1981). The local turbulence produced by vehicles directly influences the heat exchanges within the canopy with modified turbulent heat exchange coefficients (Fujimoto et al., 2008; Khalifa et al., 2016; Denby et al.,2013). The vehicle body also has radiative impacts on the local environment, including decreased solar radiation received by the surface. The physics related to vehicle dynamics has been well studied, and many models have been developed to simulate their various components at different levels of complexity (Jazar, 2009), from analytical approximations (Pacejka, 2000) to extensive numerical calculations (Farroni et al., 2014). Despite the significant impact of traffic on the local scale, these tools have not yet been integrated into models that simulate local surface climate conditions.

Two classes of Land Surface Models (LSMs) are suitable for including the traffic impacts introduced before on local climate conditions: urban climate models and road weather forecast models. Built to model the local conditions of artificial environments such as cities or the road network, they are able to accurately simulate city-wide building energy consumptions (de Munck et al., 2013; Jin et al., 2021), urban heat island effect (UHI) (De Ridder et al., 2015; Lemonsu et al., 2015) or road

https://doi.org/10.5194/egusphere-2025-2777
Preprint. Discussion started: 10 July 2025

surface conditions (Colas et al., 2024). Depending on the purpose of the model, several traffic processes have been included, but they often rely on oversimplification. Urban climate models, developed mainly to study the urban climate and to provide boundary conditions to atmospheric models, only include the heat released by traffic (Lipson et al., 2024). It is modelled as a simple parameterisation of diurnal heat released directly into the atmosphere as sensible or latent heat (Lipson et al., 2024). This source is often aggregated and inseparable from the other sources of anthropic heat. Khalifa et al. (2016) have made a first attempt to model the entire set of impacts of traffic heat on snow-free roads within the urban climate model Town Energy Balance (TEB). This attempt has been largely inspired by Fujimoto et al. (2008) with the RSV-SV road weather model. Traffic impact parametrisations are more widely used in road weather models, since traffic has a significant impact on road surface conditions. NORTRIP (Denby et al., 2013), RoadSurf (Karsisto, 2024), BJ-ROME (Meng, 2018) and METRo (Crevier and Delage, 2001) road weather models include simple parameterisations of the anthropic heat released by traffic as a diurnal sensible heat flux. The RoadSurf model from the Finnish Meteorological Institute also includes a parameterisation of traffic impact on the surface hydrology, through contact of the tyre with the surface: the amount of water or snow decreases exponentially with time through the spray and splash processes. This impact is also included in the Norwegian NORTRIP model with a formulation that depends on the speed and count of moving vehicles. In addition, the NORTRIP model includes the impact on turbulent exchange between the road surface and the air with modified exchange coefficients.

In this study, a new modelling strategy introduced in Sect. 2 is developed to take into account the traffic impacts in the LSMs. This approach is mainly developed to improve road surface conditions in winter, as traffic impacts in winter are larger than in summer. It is integrated into the SURFEX-TEB V9.0 urban climate model in order to improve the simulation of winter conditions (Colas et al., 2024). Parametrisations are developed for the heat released from engine inefficiencies and the surface-tyre interaction, impact of the vehicle body on the radiation budget, and impact on the turbulent heat exchange as presented in Sect. 3. New consistent formulations are derived from approximated analytical solutions that depend on vehicle density. The heterogeneity of the driving behaviours and vehicle models are also estimated and taken into account. This new parametrisation is evaluated at two locations chosen in Southern Finland, at road weather stations with atmospheric, surface, and vehicle counting observations. These experiments and the configurations of the model TEB are detailed in Sect. 4. The SURFEX-TEB V9.0 model with traffic impacts is then evaluated against road surface observations Sect. 5. Finally, Sect. 6 discusses the results of our modelling before the concluding remarks.

2 Modelling strategy

2.1 Including traffic impact parameterisations in TEB

In this article, TEB is improved with new parameterisations. The model will now take into account the heat released from engine inefficiencies, the impact of the vehicle body on the radiation budget and on the turbulent heat exchange, and the heat produced by the surface-tyre interactions, as shown in Fig. 1. The direct impacts of traffic on the water, ice, and snow cover are not modelled. They do not fall in the scope of this study. As TEB is an horizontally averaged model, the model must integrate

https://doi.org/10.5194/egusphere-2025-2777
Preprint. Discussion started: 10 July 2025

horizontally averaged traffic impacts. So, for example, at one model grid point, despite the significant heterogeneity of the road traffic, the wind induced by the entire vehicle fleet returns a single horizontal average value.

Two different energy budgets are modelled in the parameterisation: the internal energy budget and the vehicle body energy balance. The latter calculates the radiation impacts on the vehicle and, conversely, the impacts of the vehicle body on TEB energy balance. The former calculates the different factors of the internal energy balance of a moving vehicle. The energy generated from the fuel combustion is transformed into mechanical energy or into heat. From the mechanical energy, a share is transferred to the road through the surface-tyre interaction. From the energy transformed into heat, the first share is released as sensible and latent heat into the air and the second share warms the bottom vehicle body as shown in Fig. 1. The different shares are estimated through the dynamics of a vehicle, modelled by a simple Newtonian mechanics equilibrium equation inspired by Bera (2019). The internal energy budget and the vehicle body energy balance are coupled through the energy used to warm the bottom vehicle body. The temperature of the bottom vehicle body surface is prescribed as in Fujimoto et al. (2008) and increases the infrared radiation emitted by the surface. To keep the coupling simple, the additional energy that increases the infrared radiation emission from the bottom of the vehicle body is provided from the internal energy balance of a vehicle. For electric vehicles, their energy efficiencies are much larger (Weiss et al., 2020). Thus, their impacts can be parameterised in the total vehicle fleet impact by simply considering no energy loss from their internal energy balance. In practice, this means multiplying the heat released as sensible and latent heat into the air and the infrared radiation from the warm surface of the bottom vehicle body by the proportion of non-electric vehicles. Finally, the turbulent heat exchange coefficient between the road surface and the air is modified by the traffic-induced wind. A simple analytical formula is developed to calculate the wind induced by traffic inspired by the study of Eskridge and Hunt (1979).

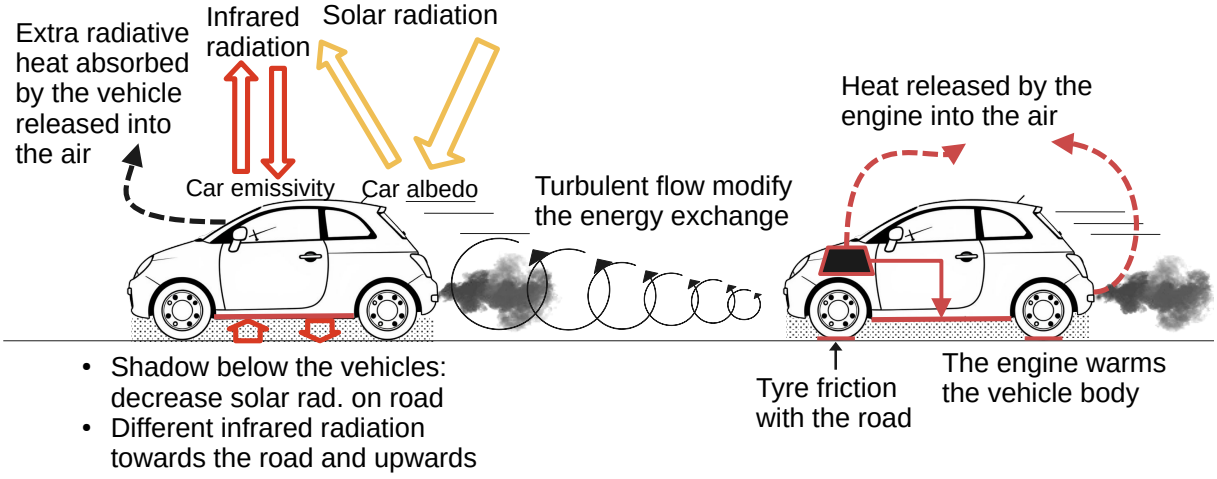

Figure 1. Simplified scheme of the traffic impacts parametererised included in the TEB model with on the left the processes related to the impact of the vehicle body and on the right the processes related to the internal operation of a vehicle

https://doi.org/10.5194/egusphere-2025-2777
Preprint. Discussion started: 10 July 2025

2.2 Traffic heterogeneity modelling within the parameterisations

Traffic impact on the local climate must be estimated considering the large heterogeneities of the vehicle type, size, internal parts, engines, and driver behaviour. On one hand, traffic is a collection of vehicles with various characteristics: size, shape, internal parts, and engine type. From the distribution of all existing characteristics of the vehicles, a finite set of variables and parameters is defined. The inherent physical characteristics of a vehicle can be defined by its weight m (kg), length l (m), width w (m), cross-section A (m^2), energy power efficiency η, and drag coefficient C_d. They are assumed to be the characteristics of a vehicle that influence the most the traffic impacts on local climate. On the other hand, at each location, traffic is a collection of driving behaviours, which can range from economical (with slow accelerations) to more aggressive. This variability in behaviour is modelled by the speed v and the acceleration a of a vehicle.

The vehicle characteristics are assumed to be independent from the driver behaviour. This assumption is reasonable, as most vehicles can reach the maximum speed allowed in all countries. However, energy power efficiency cannot be assumed to be independent from the driver behaviour: engine efficiency η_e depends directly on speed, acceleration, gear choice and engine type. Thus, the following assumptions are made: (1) The distribution of vehicle body characteristics is specified through its average values ($\overline{m}$, $\overline{l}$, $\overline{w}$, $\overline{A}$, $\overline{C_d}$) as shown in Fig. 2. They are independent from the other variables and represent a vehicle that has the average characteristics of the overall automobile fleet. (2) An average vehicular speed $\overline{v}$ is measured at a specific location, but the distribution of the speed and acceleration of the vehicle fleet at this location is unknown. So, the relationships between $\overline{v}$ and the distribution the of speed and acceleration are inferred from other data sources. They are then inserted into the traffic impact equations as explained in the next paragraph and in Appendix B to take into account the impact of the collection of driver behaviour. (3) Because instantaneous engine efficiency depends on each vehicle speed, and the vehicle fleet has a distribution of the speed, an average engine efficiency $\overline{\eta_e}(\overline{v})$ of the total automobile fleet depending on the average speed $\overline{v}$ is computed. It is estimated from other input data sources, as shown in Fig. 2.

https://doi.org/10.5194/egusphere-2025-2777
Preprint. Discussion started: 10 July 2025

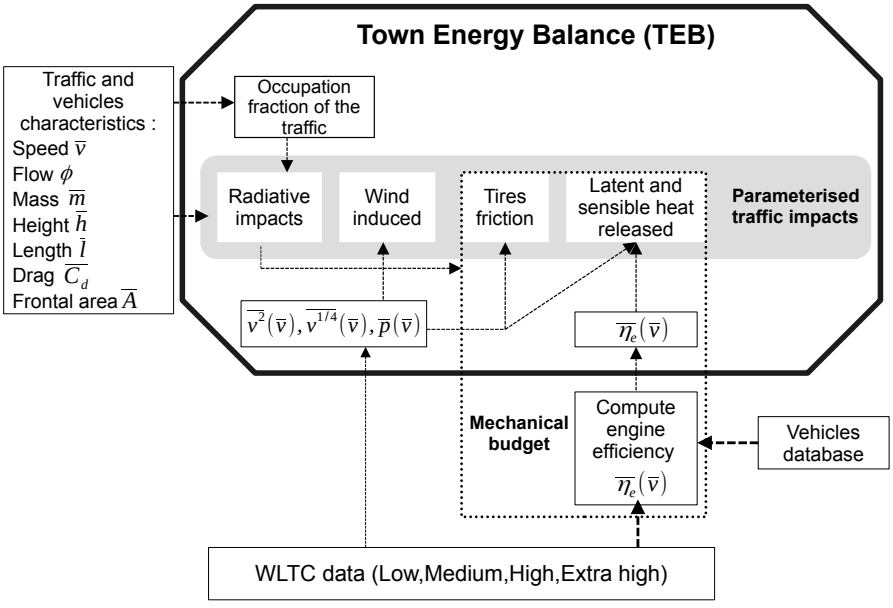

Figure 2. Protocol of the study to integrate the traffic impacts in the model TEB with the use of the World Light vehicles Test Cycles (WLTC) data

The collection of driver behaviour and its impact on traffic impact is estimated using the Worldwide Harmonised Light vehicles Test Cycles (WLTC). These cycles have been designed to provide a common and reliable measure of the energy consumption of all vehicles sold in the European Union. Since 2019, for every vehicle sold, car manufacturers have the legal obligation to provide detailed vehicle energy consumptions measured with the WLTC. For passenger cars, researchers designed four subcycles, $s = \{1, 2, 3, 4\}$, of low-speed, medium-speed, high-speed, extra-high speed representative of different road types. In this study, these cycles are considered to be associated with urban areas, suburban areas, rural areas, and highways, respectively. Each WLTP cycle has been built from a speed and acceleration data sample of the world's driving habits (Tutuianu et al., 2015).

3 Methods

In TEB, the area occupied by each component (buildings, gardens, snow-cover) is defined by an occupation fraction. The same strategy is used for the traffic. Vehicles cover a fraction of the road area f_{traff}. In agreement with the horizontally average modelling in TEB, f_{traff} represents the proportion of a segment perpendicular to the road covered by traffic. Vehicles are considered to drive in the snow-free part of the road only. Thus, when snow covers the road, f_{traff} is weighted by the snow fraction f_{sn} calculated as in Colas et al. (2024). With the traffic flow Φ (vehicles s^{-1}) and average traffic speed $\overline{v}$ (m s^{-1})

https://doi.org/10.5194/egusphere-2025-2777
Preprint. Discussion started: 10 July 2025

punctual measures f_{traff} is defined as:

$$f_{traff} = (1 - f_{sn}) \frac{\overline{w}}{w_{rd}} (\frac{\overline{l}}{\overline{v}} \Phi) \quad (1)$$

with $\overline{w}/w_{rd}$ the lateral occupation of the road traffic calculated with w_{rd} the road width and $\overline{w}$ the average vehicle width and $\overline{l}$ the average vehicle length.

3.1 Traffic impact on the radiative budget

Each vehicle is modelled as a flat 2-side surface, each with a different surface temperature. The upper vehicle body temperature is modelled equal to the air temperature T_{can} (K) of the lower air layer of TEB. The bottom vehicle body temperature warmed by the vehicle engine is modelled as in Fujimoto et al. (2008) equal to $T_{can} + 22.5K$. In addition, vehicles are modelled as a new component at ground level which shade the road, contributes to infrared emissions and radiation inter-reflections within the canyon calculated as in Lemonsu et al. (2012). Immersed in the urban canyon of TEB, the traffic takes part in the radiative exchange with the other TEB components: road, walls, windows, ground-based vegetation, and tree canopy. The footprint of traffic impact on energy exchanges is assumed to be strictly equal to the total area occupied by the vehicle fleet. Thus, each vehicle impact on the TEB energy exchanges is aggregated with the traffic occupation fraction f_{traff}, which represents the entire vehicle fleet.

The vehicle body energy budget composed of the shortwave and longwave radiation is solved. In addition, each vehicle is modelled without explicit thermal capacity: it means that the extra energy from the radiative budget absorbed by the vehicle body is transferred direcly as sensible heat directly into the urban canyon air bottom layer. It is written as follows:

$$S^*_{veh} + LW^*_{veh} = H_{res} \quad (2)$$

where S^*_{veh} (W m^{-2}) is the shortwave radiation absorbed by a vehicle, LW^*_{veh} (W m^{-2}) the longwave radiation absorbed by a vehicle and H_{res} (W m^{-2}) the residual energy drive by the radiative balance excess that is transferred as sensible heat directly into the urban canyon air bottom layer.

The solar radiation received by a vehicle is modelled as the sum of three terms: the direct $S_r^{\Downarrow}$ and diffuse solar radiation $S_r^{\downarrow}$ received at the ground level and the infinite solar reflection within the urban canyon. A share of the solar radiation received by a vehicle is then reflected by the vehicle albedo α_{veh}. In addition, the reflection within the urban canyon are modified by the new aggregated surface albedo $\overline{\alpha_g}$ written :

$$\overline{\alpha_g} = (1 - f_{sn})(1 - f_{traff})\alpha_{rd} + f_{traff}\alpha_{veh} + f_{sn}\alpha_{sn} \quad (3)$$

With f_{sn} the fraction of the snow occupation on the road, α_{sn} the albedo of snow, α_{rd} the albedo of the snow-free road surface and f_{traff} the traffic occupation fractions defined Eq. (1).

The longwave exchanges are computed following a linear approximation of the Stefan–Boltzmann law as in Lemonsu et al. (2012). As for the solar radiation, TEB solves the energy budget from the infrared radiation for each component. The vehicle longwave exchange are calculated with the walls, the windows, the sky, the road and summed over to give the total

https://doi.org/10.5194/egusphere-2025-2777
Preprint. Discussion started: 10 July 2025

longwave radiation absorbed by a vehicle. Each component in TEB is also impacted by the vehicle at ground level: for each component in TEB, the additional exchange with vehicle body is added to the longwave exchanges.

3.2 Vehicle's internal heat and tyres friction

Each vehicle is an autonomous system with its own internal behaviour and physical response. It affects the physical variables of the street while passing with heat relased in the atmosphere and with heat transferred to the road surface from tyre friction. The heat relased in the atmosphere is lost from the combustion of fuel in an internal combustion engine (ICE) due to mechanical inefficiencies η_m from all the mechanical frictions and rotating parts of the vehicle and the thermodynamic inefficiencies of its engine $\eta_e(n, M)$. The product of both η_m and $\eta_e(n, M)$ gives the total instantaneous vehicle efficiency coefficient η. The thermodynamical inefficiencies of its engine depending on the engine rotation n (rpm) and torque M (N m^{-1}) are a key variable for representing the energy lost by vehicles and for tracking changes in energy performance over the years (Johnson and Joshi, 2018). The maximum engine efficiency η_{emax} can be reached with a specific engine rotation speed and torque, but most of the time the engine efficiency of the vehicle is lower. A vehicle power-efficiency can either be directly measured (Newman et al., 2015; Stuhldreher et al., 2018) or modeled to construct engine thermal maps (Bera, 2019; Newman et al., 2016; Shourehdeli et al., 2025). Simple but precise enough physics-based tools can then be used to model the entire vehicle's response to a ride for internal combustion engines (Bera, 2019; Kargul et al., 2016, Newman and Dekraker, 2016) or electric engines (Sher et al., 2021; Kargul et al., 2025). In this study, η_m is considered constant and equal to 0.90 as in Bera (2019), since its variations for every driving condition are small compared to the variations of $\eta_e(n, M)$ and an indirect estimate of η_e is developed $\overline{\eta_e}(\overline{v})$ that accounts for the driver behaviour as explained in Sect. 2.2 and detailed in Appendix B.

The vehicle dynamics and internal energy balance are modelled through a system of 4 simple equations. The vehicle trajectory is assumed to be a rectilinear motion on a road assumed to be flat. Following the simple tools developed to model the response of a vehicle, the traction force imposed by the engine on the wheels F_{trac} in newton is calculated from an equilibrium equation applied to the vehicle following the kinematics of point masses. As the other terms of the motion equation can be estimated, this allows to deduce the force, and corresponding power P_{trac}. A fraction of the oil consumed by the internal combustion engine of vehicles that deliver the power P_{fuel} in watts is transformed into mechanical power with traction power P_{trac} in watt through the total instantaneous vehicle efficiency coefficient η. The power lost due to the vehicle mechanical and thermodynamical inefficiences is then dissipated as heat $P_{heat\,loss}$ in watts. This system is written:

$$\begin{cases} m\frac{dv}{dt} & = F_{trac} - (F_r + F_{aero}) \\ P_{trac} & = vF_{trac} \\ P_{trac} & = \eta P_{fuel} \\ P_{heat\,loss} & = P_{fuel} - P_{trac} \end{cases} \tag{4}$$

with v (m s^{-1}) the vehicle speed, F_r in newton, the rolling friction force, and F_{aero} in newton the aerodynamical drag force. F_{aero} is expressed as usual for vehicle kinematics corresponding to high Reynolds number, and the rolling friction force F_r is

https://doi.org/10.5194/egusphere-2025-2777
Preprint. Discussion started: 10 July 2025

expressed following Bera (2019) and Jazar (2009) as an empirical formula valid for a 4-wheel passenger car:

$$F_r = mg(8 \times 10^{-4}(5.1 + \frac{5.5 \times 10^5 + 90mg}{p_t} + \frac{1100 + 0.0388mg}{p_t})v^2) \quad (5)$$

$$F_{aero} = \frac{1}{2}\rho C_d A v^2 \quad (6)$$

With p_t (Pa) the tyre pressure, m (kg) the vehicle mass, g (m s^{-2}) the gravity constant, ρ (kg m^{-3}) the air density, C$_d$ the drag coefficient and A (m^2) the frontal area of a vehicle.

Then three strategies are used to parameterise the heat transferred to the road surface from tyre friction, and the heat relased in the atmosphere. First, in the model, it is assumed that the rolling resistance is fully converted as heat flux to the road surface. Indeed, the constraining forces acting against the vehicle force produced (F_{trac}) also contribute to the heat transferred to the environment. The rolling resistance acts as a mechanical constraint on the tyres and the road, part of which is dissipated as heat. Since the tyre temperature, the heat transfer coefficient, the amount of energy transferred to the tyre and the road, and the amount of energy directly converted into heat are unknown, the rolling resistance power $P_r = F_r v$ is fully converted as heat flux to the road surface.

Then, a part of the power dissipated as heat $P_{heat\ loss}$, calculated with Eq. (4), is used to warm the bottom vehicle body at temperature T_{veh} as explained in Sect. 2.1. It increases the infrared radiation emitted to the road surface $LW^{\downarrow}_{veh \to rd}$ (W m^{-2}) because of the warmer bottom vehicle body surface. So, starting from the bottom of the vehicle body in thermal equilibrium with the environment at T_{can} (K), the power P_{lw} (W m^{-2}) to reach the infrared radiation emitted at temperature T_{veh} (K) is:

$$P_{lw} = LW^{\downarrow}_{veh \to rd}(T_{veh}) - LW^{\downarrow}_{veh \to rd}(T_{can}) \quad (7)$$

This power is then taken from the total heat produced by the vehicle $P_{heat\ loss}$.

Finally, to take into account the effects of the vehicle system in the TEB model, these effects are then aggregated for the entire traffic with a traffic flow Φ (vehicles s^{-1}) and an average traffic speed $\overline{v}$ (m s^{-1}). In addition, the large heterogeneity of vehicle characteristics and behaviour is taken into account in these previous equations with the methodology explained in Sect. 2.2 and described in Appendix B through regression equation estimates ($\overline{v^2}(\overline{v})$, $\overline{p}(\overline{v})$, $\overline{\eta_e}(\overline{v})$, $\overline{a}$) of $\overline{v}$ and vehicle fleet average characteristics ($\overline{m}$, $\overline{l}$, $\overline{w}$, $\overline{A}$, $\overline{C_d}$).

So, the heat transferred to the road surface from tyre friction is modeled through the rolling resistance power averaged over the vehicle surface S_{veh} (m^{-2}) for the entire vehicle fleet Q_r in watt per metre squared written:

$$Q_r = f_{traff}\frac{F_r(\overline{v})\overline{v}}{S_{veh}} \quad (8)$$

In addition, the power dissipated as heat $P_{heat\ loss}$ released in the atmosphere over each vehicle surfaces S_{veh} (m^{-2}) for the entire vehicle fleet averaged in watt per metre squared Q_l is written:

$$Q_l = f_{traff}\frac{P_{heat\ loss}(\overline{v})}{S_{veh}} - f_{traff}P_{lw} \quad (9)$$

https://doi.org/10.5194/egusphere-2025-2777
Preprint. Discussion started: 10 July 2025

Q_l is then transformed as a source of sensible and latent heat flux using the formulation of Pigeon et al. (2007):

$$H = 0.92 Q_l \tag{10}$$

$$LE = 0.08 Q_l \tag{11}$$

3.3 Modification of the turbulent heat exchange with the road surface

The collection of vehicles driving on a street immersed in an urban canyon has direct effects on the physical variables of the environment. The physical body of a vehicle is an obstacle that induces drag, increases fluid velocities, and turbulence. Turbulence plays a key role in the boundary layer. It leads to heat and moisture exchange between the air layer and the different surfaces. In this study, only the influence of traffic on the road surface and the lower air layer is considered. Thus, the turbulent exchange coefficient between the road surface and the first air layer is modified by the traffic impact in the model.

Each vehicle is considered to be an independent system. The air motion triggered by a moving vehicle can be described using three regions: along the sides of the vehicle, in its near-wake, and in its far-wake. In the first area, the fluid flow is assumed to be laminar to prevent extensive calculations. From the Navier-Stokes equation, the fluid is assumed to be incompressible, without pressure forces, and to have reached a steady state. Under a vehicle, the fluid is considered to move between two infinite parallel plates with the upper one moving tangentially relative to the other. This flow is modelled as a simple linear Couette flow U_l (m s^{-1}) as shown in Fig. 3.

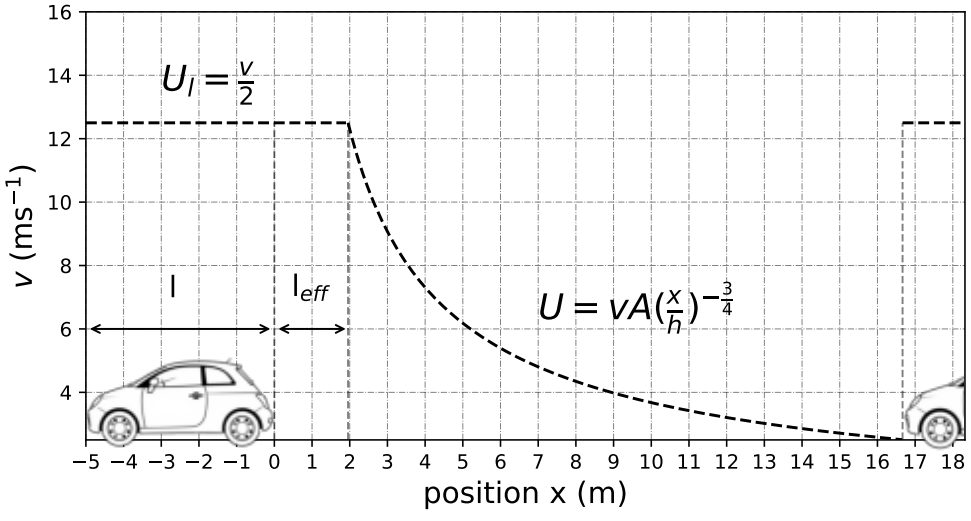

Figure 3. Schematic representation of the wind induced by a vehicle and the modelled equations on the urban canyon, with the wind-induced under the vehicle (l) on the near-wake (l_{eff}) and on the far-wake up to the next vehicle

A simple power law $U \sim x^{-3/4}$ is used to calculate the average wind induced by vehicles in the wake of a vehicle from Eskridge et al. (1979). They developed an analytical formula to calculate the longitudinal velocity field deficit U (m s^{-1}) in

https://doi.org/10.5194/egusphere-2025-2777
Preprint. Discussion started: 10 July 2025

the wake of a vehicle. They linearised the Navier-Stokes momentum equation using a perturbation analysis. This equation depends on several parameters estimated on wind tunnel experiments. The longitudinal velocity field deficit U is determined in the absence of crosswinds, stable conditions, and low natural wind velocities and is valid after a downwind distance equal to approximately ten vehicle heights h (Baker, 2001). The reader should refer to Eskridge et al. (1979) for a complete demonstration. The longitudinal velocity in the wake also depends on the other coordinates. It has been used in various studies to calculate the dispersion of pollutants in the wake of a vehicle (Eskridge and Rao, 1983; Hargreaves and Baker, 1997) and improved (Rao, 2002). The vertical and horizontal velocity components can also be calculated according to Hider et al. (1997).

Two assumptions are made to keep the wind-induced formula simple and with consistent mathematical properties: (1) It is assumed that the formula $U(x)$ is also valid in the near-wake of the vehicle (i.e x < 10h). However, a lower bound is determined (i.e x > l_{eff}) for continuity reason with the Couette flow U_l. Thus, the Couette flow is extended up to l_{eff} in the near-wake of a vehicle, then $U(x)$ is used further in the wake of the vehicle when $U(x) < U_l$. (2) Then, an average wind speed induced by the entire traffic is found $U_{traff}(\overline{v})$ (m s^{-1}) by calculating the integral along the x-axis. Each wind induced by a vehicle is considered to have no overlap from the wind induced by each vehicle. So, the average wind speed is calculated along the vehicle and in the wake until the front of the next vehicle $U_{traff}(\overline{v})$ as shown in Fig. 3. The complete demonstration is given in Appendix A.

This analytical formula $U_{traff}(\overline{v})$ has several refinements over the empirical equation from Fujimoto et al. (2008) and used by Khalifa et al. (2016). The formula $U_{traff}(\overline{v})$ depends explicitly on the vehicle height, length, speed, and traffic intensity, whereas the empirical formula from Fujimoto et al. (2008) depend on the vehicle speed only.

In TEB, the sensible and latent heat between the road surface and the air layer are calculated at ground level, and both use the wind speed at level z. So, the wind speed $U_{traff}(\overline{v})$ is vertically interpolated to the level z using the Monin–Obukhov log-wind profile under neutral conditions adjustement as:

$$U_{traff}(\overline{v}, z) = U_{traff}(\overline{v}) \frac{ln(\frac{z}{z_0})}{ln(\frac{z_{traff}}{z_0})} \tag{12}$$

With z_o (m) the road roughness length, z_{traff} the heigth of the traffic-induced wind. In this study, z_{traff} is set at mid-height of the vehicle. Contrary to Khalifa et al. 2016 , the increased turbulent exchange caused by traffic is not a new component but a direct modification of the turbulent exchange coefficients embedded in TEB. The sum of the wind components at level z gives:

$$U_{eff} = \sqrt{U_{can}^2 + (u^* + w^*)^2 + U_{traff}(\overline{v}, z)^2} \tag{13}$$

With $(u^* + w^*)^2$ (m s^{-1}) the total turbulent wind component with w^* (m s^{-1}) caused by the local canyon convection and U_{can} (m s^{-1}) the natural wind at the lower level. It is used to adjust the aerodynamic resistance of the sensible and latent heat exchange with the road surface R_{rd} calculated as in Lemonsu et al. (2012).

https://doi.org/10.5194/egusphere-2025-2777
Preprint. Discussion started: 10 July 2025

4 Experimental set-up and model configurations

This model improvement study is based on the version of the TEB model described in Colas et al. (2024), which models cold conditions using explicit modelling of snow and ice with processes of water melting and freezing. This version of TEB is used as a reference in comparison with the modified version named TEB-CAR, which includes the anthropic processes described in the previous sections. Both are compared with observations to study the physics response and the accuracy of the improved model. Southern Finland road weather stations are chosen because they have both traffic and weather measurements, as shown in Fig. 4.

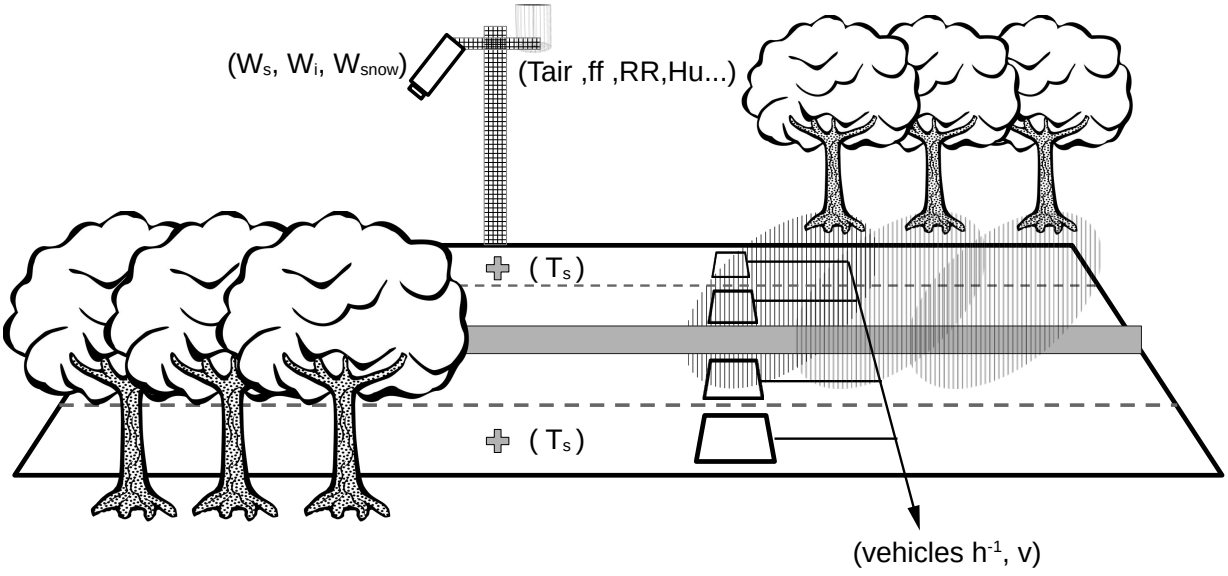

Figure 4. Schematic representation of the 2x2 highway between Turku and Helsinki with roadside trees at a weather station location installed by Fintraffic. On the roadside tower, atmospheric sensors are installed with Air temperature (Tair), wind speed (ff), precipitation (RR) and optical surface conditions sensors, ice (W_i), snow (W_{snow}), water (W_s). On the busy lanes, surface sensors measure road surface temperature (T_s), and traffic counting systems measure the number of vehicles and the vehicle speed v.

Measurements of paired traffic and physical variables are essential for this study, as well as long data series with robust road surface temperatures in busy road lanes. Nupuri (60.22805N, 24.59641E) and Palojärvi (60.29328N, 24.31916E) road weather stations are chosen among the road weather stations deployed on the Turkü-Helsinki highway because a strong car commuting pattern is observed at these stations. The majority of the commuters go to Helsinki in the morning, then drive home creating clear differences of the road surface physical variables between both directions. It allows to isolate the traffic impact from the other effects since both directions are subject to the same atmospheric conditions. This study takes advantage of this commuting pattern to evaluate the TEB-CAR capacity to model the marginal effects of traffic impacts at these road weather stations.

https://doi.org/10.5194/egusphere-2025-2777
Preprint. Discussion started: 10 July 2025

These stations manufactured by Vaisala measure common atmospheric variables from roadside towers such as air temperature, wind direction and speed, humidity, precipitation, and also road surface conditions. Water, ice and snow on the road are measured by optical sensors and road surface temperature is measured with asphalt embedded sensors. These physical variables are directly influenced by the effects of traffic and winter maintenance operations with large impacts on the road surface conditions. Road temperature sensors are buried under one high-speed lane for each direction. In addition, Fintraffic installed a vehicle counting system several kilometres ahead in each lane. These measurements are available as the Zenodo dataset attached to this study (Colas, 2025).

Every 6 minutes, atmospheric observations are transformed into hourly measurements to force the TEB and TEB-CAR models. To calculate hourly values, the value closest to the full hour is extracted. The 6-minute accumulated precipitation measurements are aggregated every full hour. Snow and rain are discriminated using the following criterion: If the air temperature is > 1 °C, the precipitation is deemed to be liquid, otherwise it is classified as snow as in Colas et al. (2024). The ERA5 reanalysis of the shortwave and longwave data at ground level is also used to force the model by selecting the grid point closest from the Nupuri and Palojärvi locations. Hourly traffic data, composed of vehicle counts and speed, are extracted from the Fintraffic API at the same location. TEB-CAR simulations are run for each direction of the road, with their associated vehicle counts every hour. The traffic counts from the slow lanes, for each direction of the road, are used to force the models because the probe embedded in the asphalt is located in the slow lanes of the pavement. Thus, in this study, it is assumed that traffic on the faster lanes has no effect on the conditions of the slower lanes. The simulation results are then compared with the local observed road surface temperatures in both directions. The closest observed surface measurements are taken from the full hours.

Simulations are done when observations are available. A joint two-month and half observation period is available at both the Palojärvi and Nupuri locations between 19 October 2017 and 30 December 2017. In addition, a longer simulation is performed at Nupuri location with more available observations from 19 October 2017 to 1 May 2018. This extended simulation is used to analyse the TEB-CAR results in Fig. 8 and Fig. 8 where the whole period is divided into two. The first period has lower solar radiation from 19 October 2017 up to 12 March 2018 (winter), and the second period has a higher maximum daily temperature and higher downward solar radiation up to 1 May 2018 (spring).

Both models are configured as the TEB-ES version in Colas et al. (2024) except for some changes to the snow removal parameterisation: the total snow cover is removed whenever the snow has been continuously present on the ground for 6 hours, except at night between 0 am and 5 am. Six levels are taken for the surface boundary layer option (Masson and Seity, 2009) for both models with T_{can} (K) the lower air temperature simulated at 0.5 m. In addition, the methodology introduced in previous sections is adapted for the specific Nupuri and Palojärvi environment in TEB-CAR. Since the surface temperature probe is embedded close to the track lane, the vehicle to road width ratio $\overline{w}/w_{rd}$ is set to 1 in the traffic fraction occupation f_{traff}. Also, the area of effect of the power dissipated as heat $P_{heat\,loss}$ through the vehicle inefficiencies released as heat into the atmosphere is modified. Although it is simple to define for dense road networks such as found in cities (Pigeon et al., 2007), depending on the model's grid length, it is more difficult for isolated roads. Rather than being dissipated only in the area corresponding to the vehicle area, it is dissipated in a S_{area} area of 100 m x 100 m as in Pigeon et al. (2007). So in Eq. (9)

https://doi.org/10.5194/egusphere-2025-2777
Preprint. Discussion started: 10 July 2025

Parameter	Values
Vehicle length $\overline{l}$	4.3 m
Vehicle cross-section $\overline{A}$	2.5 m^2
Vehicle tire pressure $\overline{p_t}$	2.3 bar
Vehicle heigth $\overline{w}$	1.8 m
Vehicle mechanical efficiency η_m	0.90
Vehicle mass $\overline{m}$	1500
Vehicle drag coeff. $\overline{C_d}$	0.56
Vehicle albedo α_{veh}	0.75
Vehicle emissivity ϵ_{veh}	0.80
Nupuri Turku avg. speed	27.70 m s^{-1}
Nupuri Helsinki avg. speed	28.03 m s^{-1}
Palojärvi Turku avg. speed	27.70 m s^{-1}
Palojärvi Helsinki avg. speed	27.70 m s^{-1}

Table 1. TEB-CAR traffic parameters and average speeds at the Palojärvi and Nupuri sites. Parameters with overlines are estimated from ICCT (2023)

$S_{veh} = S_{area}$ and $\overline{l} = 100\ m$ inside f_{traff}. Finally, the input traffic parameters for the TEB-CAR simulation are derived from the average characteristics of the Finland vehicles in 2018 from ICCT (2023) as displayed in Table 1.

In Sect. 5.2, an ablation setup is implemented. It means that besides the reference simulation of TEB-CAR, 4 more simulations are done, each with a traffic impact removed from the model. They are named rolling friction, heat lost, radiative, and wind-induced. By removing a traffic impact for each simulation it is possible to investigate its relative impact on the simulated variables in comparison with the reference simulation of TEB-CAR.

5 Evaluation at Nupuri and Palojärvi locations

5.1 Performances of the traffic impacts parameterisations

A significant commuting pattern is observed at the Nupuri and Palojärvi road weather stations during the simulation period, with an average of 1200 and 1100 vehicles per hour, respectively, during morning peak hours towards Helsinki and 1000 and 800 vehicles per hour, respectively, in the opposite direction during the afternoon. The time series shown in Fig. 5 gives insights about the traffic-induced impacts throughout the simulation. It is composed of a subset period of 5 working days until the 23 December 2017 characterised by a clear commuting pattern, and of a subset period of 3 nonworking days up to the 26 December 2017 characterised by a similar traffic intensity in both directions.

https://doi.org/10.5194/egusphere-2025-2777
Preprint. Discussion started: 10 July 2025

There is a clear increase in road surface temperature (RST) simulated by TEB-CAR in both directions compared to the TEB simulation. TEB exhibits a significant cold RST bias with respect to the observations, which is corrected by the new processes integrated into the model. Even during the night, when traffic is sparse, the RST is higher due to the strong heating effects throughout the day. This effect can be highly relevant given that dangerous conditions for drivers occur more frequently in the morning with a lower RST reaching freezing temperatures. In addition, the TEB-CAR simulations accurately follow the observed RST in both directions in Fig. 5 in terms of trend and maximum or minimum.

One should confirm that the bias reduction is not coincidental with other potential biases such as sensor bias. So, the temperature difference caused by the commuting pattern between the two lanes is used to verify the accuracy of the traffic-induced effects modelled in TEB-CAR. In Fig. 5, the TEB-CAR RST differences match the observed RST amplitude. The strongest RST differences during peak hours, especially in the morning, are well reproduced by TEB-CAR. The traffic difference is lower in the afternoon than in the morning, as seen in the graph, which imply lower RST difference amplitudes well reproduced TEB-CAR.

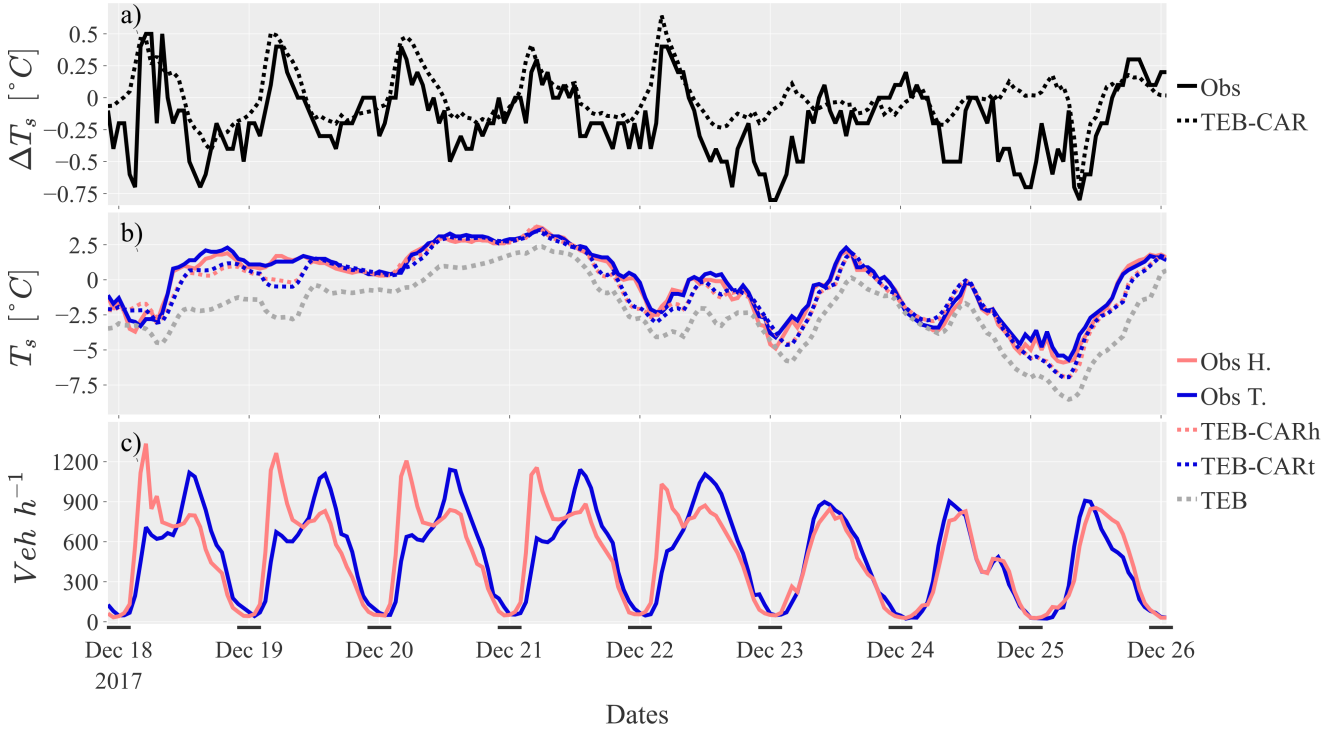

Figure 5. Comparison between TEB and TEB-CAR model version simulations (TEB-CARh for the simulation toward Helsinki and TEB-CARt for the simulation toward Turku) on a 8-days subset period from monday to tuesday one week later with the observations measured at Nupuri location. From top to bottom panel : (a) observed and modelled road surface temperature difference, (b) road surface temperature, (c) number of vehicles per hour

https://doi.org/10.5194/egusphere-2025-2777
Preprint. Discussion started: 10 July 2025

The RST differences between the two directions are analysed more precisely in Fig. 6. During weekends, traffic intensity differences are smaller as shown in Fig. 5. Thus, traffic impact differences are also smaller with lower ΔT_s. There is no clear pattern with the traffic intensity differences in the observed ΔT_s while there is in the ΔT_s simulated. During working days wekdays, the traffic intensity differences are much bigger as the ΔT_s for both observed and simulated values. The $\Delta Traffic$ distribution is positively skewed at both locations during working days with values mostly between 0 and -250 vehicles h^{-1}. Natural factors and road energy inertia have a direct impact on the RST with scattered simulated values around the regression line. The RST heteroscedasticity for the higher $\Delta Traffic$ suggests that the natural factor and the traffic-induced effects are more intertwined for higher traffic intensities.

Consistency is found between the simulated and observed traffic-induced effects with almost equivalent slopes between observed and simulated RST differences from the robust linear regressions (RLM) (Huber, 1973), designed to be robust to outliers. Also, regression equations for both at Nupuri and Palojärvi location have the same slope depending on if its calculated on observations or simulations. So there is a consistent behaviour of the traffic impact on TEB subject to different traffic patterns and atmospheric conditions. The TEB-CAR simulations accurately represent the traffic differences impact up to 750 vehicles per hour. At Nupuri location, observed and simulated RST differences distributions are shifted, the intercept of the regression equation for observed RST differences is negative and observed RST differences have a cold bias. These markers suggest that there is elements that produce this cold bias at Nupuri location that are not taken into account in TEB-CAR. It can also suggests that there is a sensor bias at this location since this effect is not found at Palojärvi location.

Using the RST differences between two road directions subject to the same atmospheric conditions is relevant to extract the traffic impact on the road from natural factors. It also allow to evaluate modelling tools that include traffic impact parameterisation. In addition, the traffic impact parameterisation in TEB-CAR correctly reproduces the traffic impact at Nupuri and Palojärvi locations with a similar regression equation slope between observed and simulated RST differences.

5.2 Analyses of the traffic impacts parameterisations

The cumulative effects of each vehicle simulated by TEB-CAR result in marked impacts on the physical variables of the road. This impact changes depending on atmopsheric conditions. But in the traffic impact parameterised in the model, some may have opposite effects or larger impacts on the physical variables and lead to different outcomes on the overall traffic impact at the local scale.

The first key result shown in Fig. 7 is that winter, on average, traffic increases the RST, whereas in spring, it decreases the RST on average. This is clear when comparing the TEB and TEB-CAR simulations in Fig. 7. This same behaviour occurs in the TEB-CAR simulation in the Turku direction, as shown in Fig. 8. The Fig. 7 and Fig. 8 also show that the traffic cooling effect in spring on the RST is mainly confined after 10 h UTC, when air temperature is high and when there is high downward solar radiation.

The processes added in TEB-CAR each have a different marginal impact on the RST: the rolling friction has a strong marginal heating effect, the increased turbulence a strong marginal cooling effect and the radiative effect a small marginal cooling effect, and the heat released in the air a small marginal heating effect as shown in Fig. 8 and in Fig. 7. The competition

https://doi.org/10.5194/egusphere-2025-2777
Preprint. Discussion started: 10 July 2025

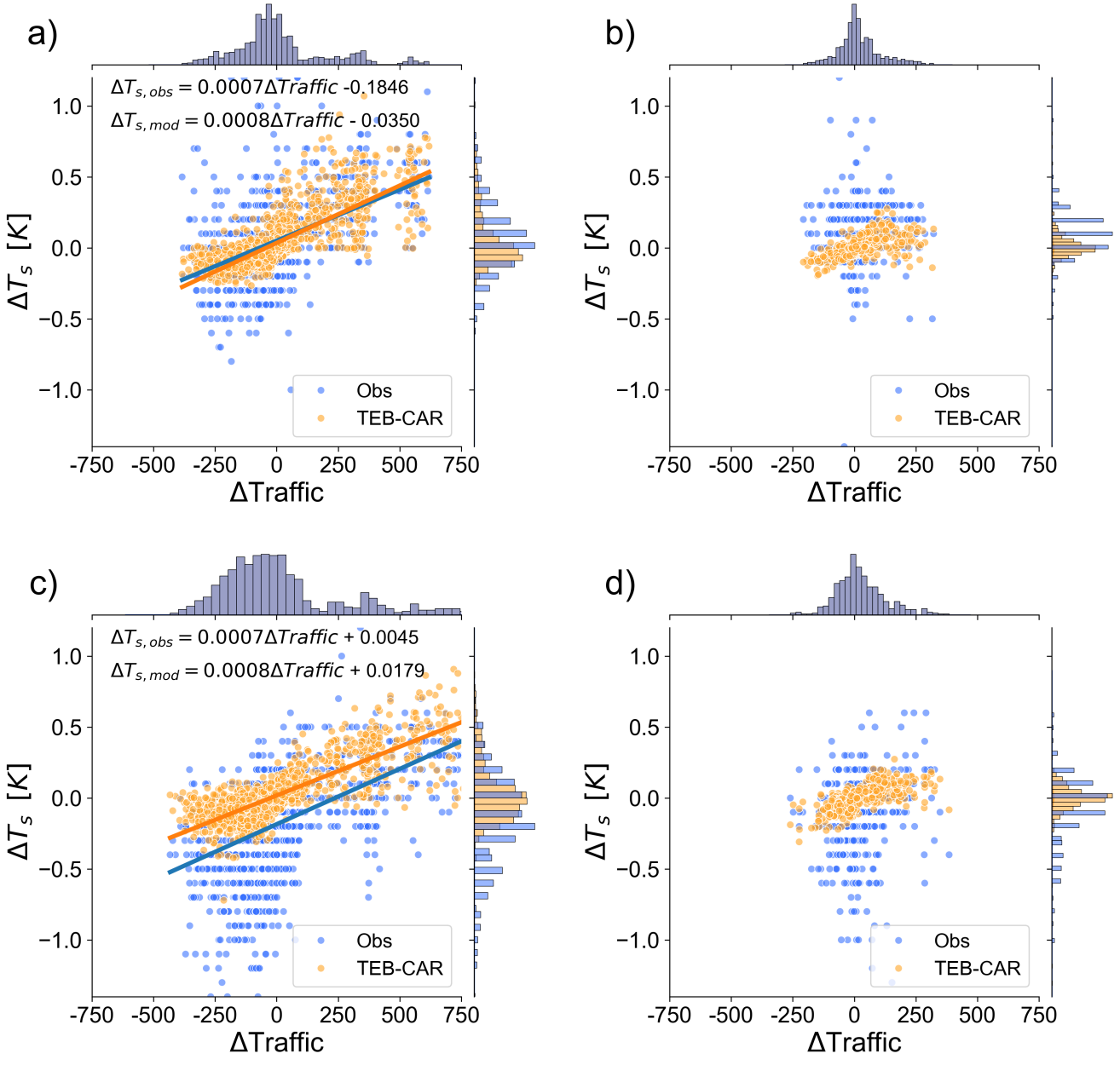

Figure 6. Simulated and observed differences of road surface temperatures ΔT_s between the Helsinki direction and Turku Direction (H-T), with robust linear regression lines (RLM) between $\Delta Traffic$ and ΔT_s. Panels (a) and (b) show the differences at the Palojärvi site on weekdays (a) and week-ends (b), respectively. Panels (c) and (d) show the same information at the Nupuri site.

on the radiative impact between the heating effect from the infrared radiation received from the vehicles and the shadowing effects from the vehicle eventually leads to an overall small cooling effect. Although this effect is small in winter, it is stronger

https://doi.org/10.5194/egusphere-2025-2777
Preprint. Discussion started: 10 July 2025

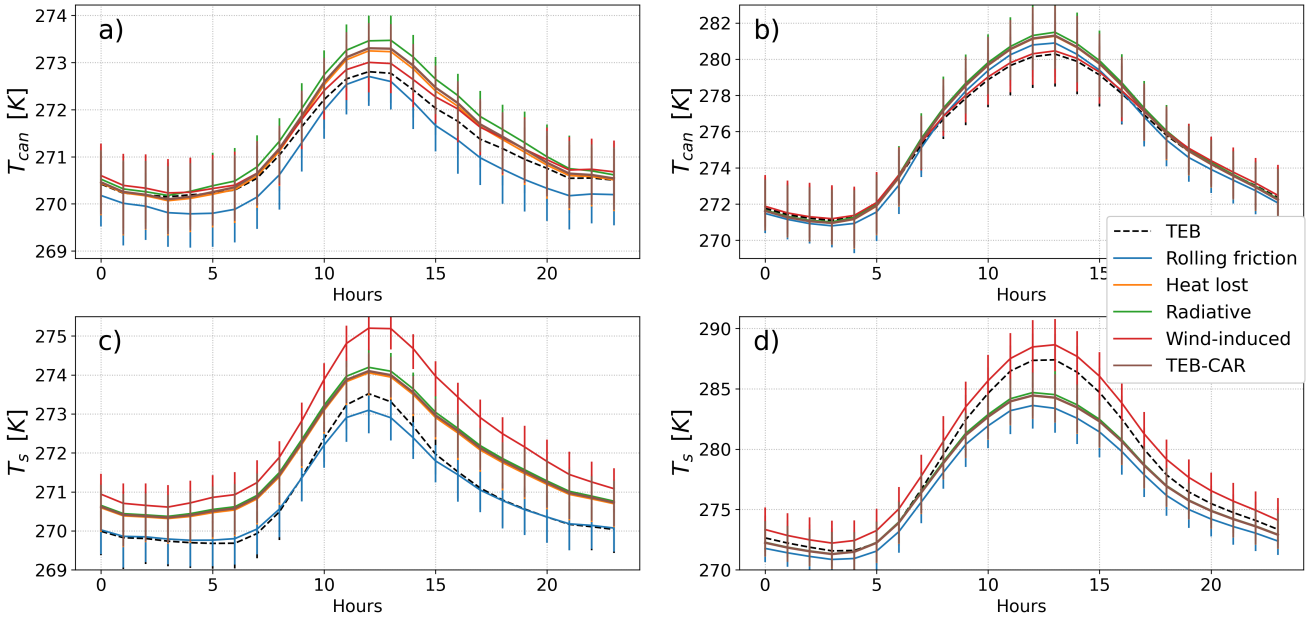

Figure 7. Simulated low air temperature T_{can} (K) (c) and (d) and road surface temperature T_s (K) (a) and (b) with the confidence interval of the estimator of the expected value with TEB-CAR and TEB models and from the ablation study implemented with TEB-CAR with one process removed at each simulation. (a) and (c) are taken on the winter period and (b) and (d) on the spring period

in spring in the afternoon with more solar radiation intercepted by vehicles than infrared radiation emitted by vehicles to the road surface, as shown in Fig. 8. Competition between all factors eventually leads to an overall heating effect on the RST in winter. This effect is significant throughout the day driven by the competition between the wind-induced impact and the rolling friction. In spring, the same competition between the wind induced and the rolling friction impacts arises. However, the wind-induced cooling effect significantly exceeds the rolling friction warming effect and leads to an overall decrease on average of the RST as previously observed.

In both periods, road traffic increases air temperature T_{can} mainly at noon, as shown in Fig. 7. Traffic-induced processes play different roles compared to the impact on RST. In particular, the effect of the traffic-induced wind plays an opposite role on the T_{can} than it does on the RST. It leads to an average warming effect on T_{can}. The marginal impact of the wind-induced impact is greater in spring than in the earlier period. The heat released by traffic has the least impact on T_{can} and on with RST on average. This phenomenon can be explained by the fact that the average heat released by traffic is low compared to the average sensible heat from the ground, as shown in Fig. B3. In comparison, the effect induced by turbulence has the greatest proportional impact on the physical variables, accounting for up to 80% of the total simulated wind at the lower level (0.5 m) in the model. Given this significant proportion, it is likely to influence other modelled variables in TEB. However, in this study, it is only considered to have an impact on the surface-air heat exchange coefficient.

https://doi.org/10.5194/egusphere-2025-2777
Preprint. Discussion started: 10 July 2025

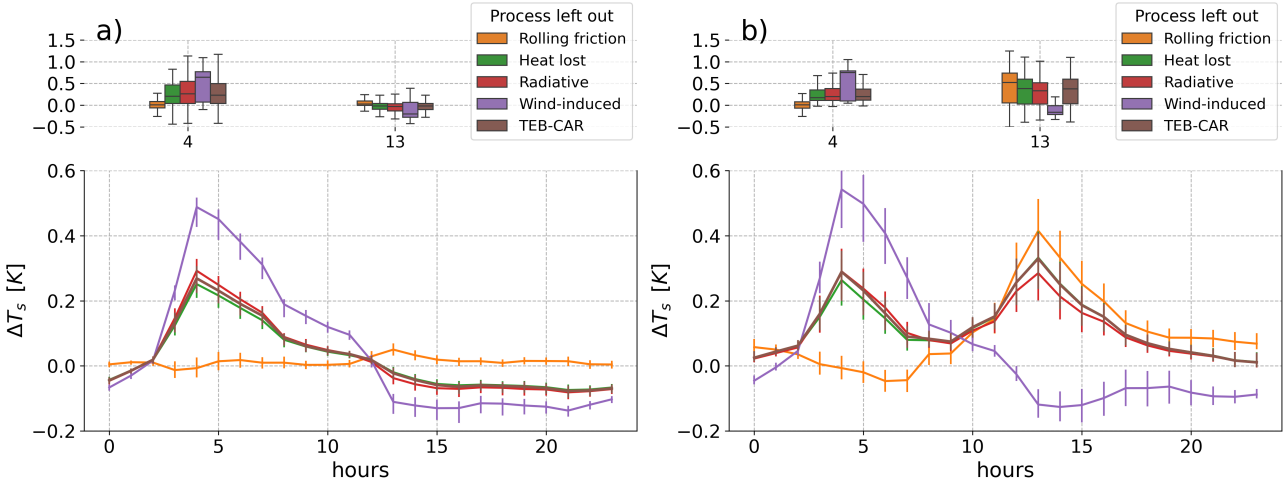

Figure 8. Ablation study of the processes implemented in the TEB-CAR with one process removed at each simulation and the reference. Road surface temperature differences (ΔT_s) with the boxplots at peak traffic intensity (4:00 h UTC and 13:00 h UTC) between the simulations and the observations for winter (a) and spring (b) with the confidence interval of the estimator of the expected value .

The rolling friction has a significant impact on the surface energy balance, with a larger impact when solar radiation is lower as shown in Fig. 8. Peak values of up to 40 W m^{-2} can be reached during intense morning traffic in the Helsinki direction and account for 40% of the total energy absorbed/received by the road surface. With respect to the heat released by internal combustion engines, its amount is relatively small compared to the total sensible heat from the surface. A significant part of the heat lost by the engine is used to warm the bottom of the vehicle body as shown in comparison with the total heat lost by the vehicle engine in appendix Fig. B3.

6 Discussion and conclusion

In this study, we introduced and evaluated a new modelling strategy to account for the traffic-induced impacts in the SURFEX-TEB V9.0 urban climate model. The approach integrates parametrizations for heat released from engine inefficiencies, vehicle body impacts on the radiation budget, turbulent heat exchange, and surface-tyre interactions, all modelled as coherent analytical solutions dependent on vehicle counting. The heterogeneity of driving behaviours and vehicle models was also considered, enhancing the model's realism. The modified model, termed TEB-CAR, was evaluated against observations from two road weather stations in southern Finland, Nupuri and Palojärvi, which exhibit strong commuting patterns. This setup has allowed to extract the traffic-induced effects from other environmental factors, as both road directions experience similar atmospheric conditions. Finnaly, we analysed the marginal impact of one traffic impact parameterised in the model.

This study demonstrates that traffic has a significant impact on road surface temperature (RST), even for a road with a medium traffic intensity as found in Khalifa et al. (2016). If one can measure the road conditions of two or more roads lanes

https://doi.org/10.5194/egusphere-2025-2777
Preprint. Discussion started: 10 July 2025

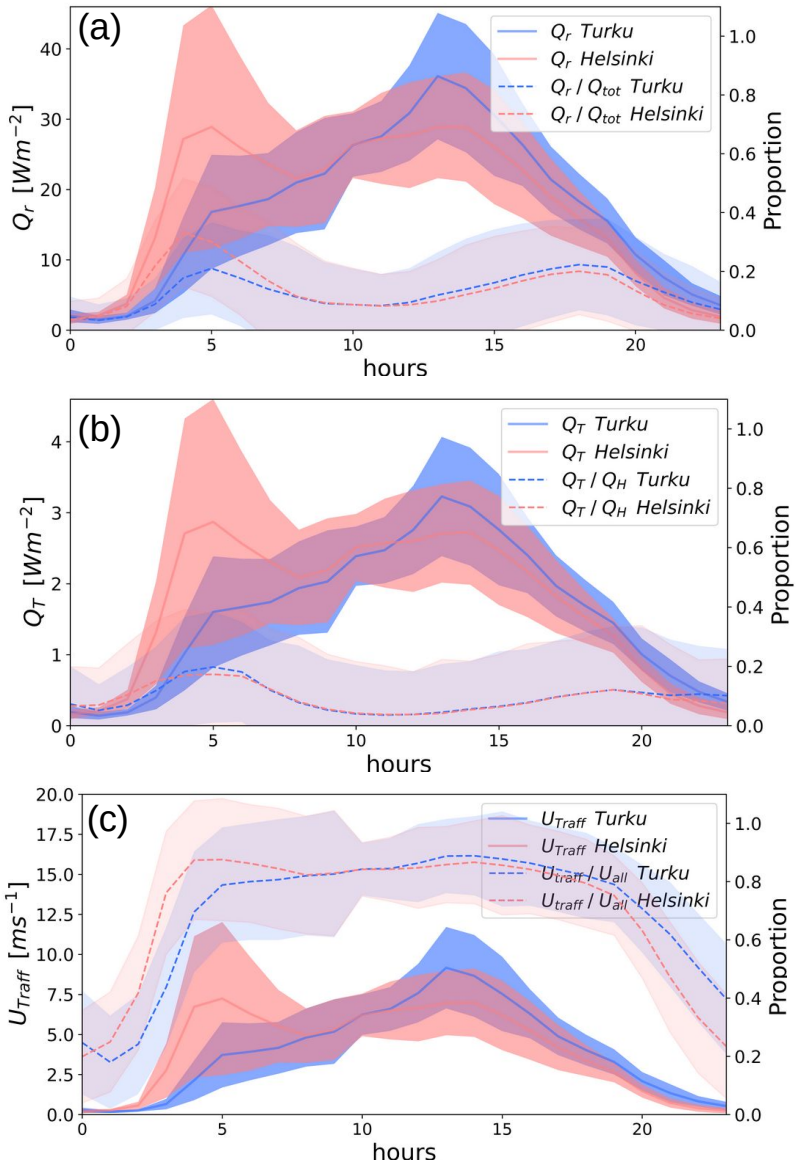

Figure 9. Diurnal traffic-induced effects in the TEB-CAR model on the whole simulation period for the Nupuri experiment with the propotion of total fluxes (a) Rolling friction and its marginal amplitude on the total heat transfered to the road Q_{tot}, (b) sensible heat released in the atmopshere and its marginal amplitude on the total sensible heat released in the atmopshere Q_H, (c) Wind-induced and its marginal amplitude on the total wind on the lower layer of the atmosphere U_{all} at 0.5 m.

with different traffic patterns, it is possible to extract the traffic-related impacts from natural factors. This methodology allows to evaluate the parameterisations of the traffic impacts in models as in road weather forecast or urban climate. TEB-CAR significantly improves the simulation of the road surface temperature (RST) compared to the reference TEB model. Compared

https://doi.org/10.5194/egusphere-2025-2777
Preprint. Discussion started: 10 July 2025

to the observed RST differences between both directions at Nupuri and Palojärvi location, TEB-CAR is able to reproduce the observed trend caused by differences in traffic intensity. In addition, depending on the atmosphere conditions, the magnitude, timing, and trend of road traffic impacts on the local climate change. It leads to increased RST for low air temperature and solar radiation, and decreased RST for higher air temperatures and solar radiation.

This study shows that taking into account the full set of impacts of the traffic is relevant to simulate road conditions and the physical variables of the atmosphere. In particular, the competition between the two major effects, the rolling resistance and the wind-induced by the vehicles is the most important characteristic of the traffic parameterisation in this study. On the contrary, the heat lost from the fuel combustion released as sensible and latent heat in the atmosphere has the least significant impact on both RST and lower layer air temperature T_{can}. So, simulating the impact of road traffic on local climate with a simple aggregated source of heat released in the atmosphere (Bohnenstengel et al., 2013; Pigeon et al., 2007; Iamarino et al., 2011) may not be enough to capture the full extent of the traffic impacts. This estimate calculated in Pigeon et al. (2007) or in Sailor and Lu (2004) is of the same order as the one calculated in this study as described in appendix B.2. This flux is small in comparison with the total heat flux released from the road surface, especially when solar radiation is high, as shown by Bohnenstengel et al. (2013) and in this study. In addition, the results of this study are consistent with those of Khalifa et al. (2016) who shown that this strategy is approriate to simulate these effects on the RST. With a RST of several degrees higher with the traffic impacts it influences significantly the forecast of dangerous road conditions.

Some road traffic impacts are overlooked in this study. The current traffic-induced effects do not take into account road conditions, such as water, ice, slush, or snow, which could significantly alter the dynamics of surface-tyre interactions. Also, the study did not explicitly consider the impact of heavy vehicles, which despite being a small percentage of the traffic could have a significant impact on RST due to their larger size and weight. Finally, the traffic intensity of the Helsinki-Turku highway is moderate compared to that observed on the main urban ring roads (Amato et al., 2016). Future work should evaluate the model subject to higher traffic intensities to assess the reliability of the traffic impacts parameterisation. The simulation period was relatively short and only two road weather stations have been used to assess TEB-CAR improvements. A more thorough evaluation would provide a stronger confidence in these parameterizations and in the model performance across different traffic patterns. It would also be relevant to assess the overall impact of traffic on the urban climate.

Despite these limitations, TEB-CAR represents a significant step forward in explicitly taking into account the traffic-induced effects on the road surface conditions and on the physical variables of the atmosphere. The model capacity to capture the impact of traffic, particularly during peak commuting hours, has a potential to improve road safety and maintenance operations in winter. Moreover, the TEB-CAR version has shown strong improvements in simulating road surface temperatures. Future research should focus on refining the parameterisations, extend the evaluation to more diverse and high-traffic environments, and to include additional factors such as the direct traffic effects on slippery conditions. This would further validate the robustness of the model and increase its applicability to different settings.

https://doi.org/10.5194/egusphere-2025-2777
Preprint. Discussion started: 10 July 2025

Appendix A: Detailed calculations of the wind induced by the traffic

An analytical formula is found to model the wind induced by the traffic U_{traff} which is integrated into the TEB model. To model the fluid velocities induced by a vehicle, three areas are considered: along the length of a vehicle, in the near-wake of a vehicle, and in the far-wake of a vehicle.

First, the velocity of the fluid under the vehicle is determined. The fluid is assumed to be incompressible, the pressure forces are considered negligible, and the steady state is found so that the partial derivative of the fluid speed U_l to time is null. Under a vehicle, the fluid is considered to be between two infinite parallel plates with the upper one moving tangentially relative to the other. Thes Navier-Stokes momentum equation simplify to:

$$\frac{d^2U_l}{dz^2} = 0 \tag{A1}$$

For $z = 0$ the road surface and the boundary conditions $U_l(0) = 0$ and $U_l(h) = v$ with v the vehicle speed. The exact solution gives:

$$U_l = v\frac{z}{h} \tag{A2}$$

So, the average wind speed between the road surface and the bottom of the car body at the heigth h yields:

$$U_l = \frac{v}{2} \tag{A3}$$

Then, the formula from Eskridge et al. (1979) is used to determine the wind speed produced in the wake of a vehicle. Eskridge et al. (1979) determined that beyond the recirculation region (x < 10h) and for (u, v, w $\leq$ v_{car}) it is possible to linearise the Navier-Stokes momentum equation with the perturbation analysis. The exact solution of the longitudinal wind speed deficit in the wake of a vehicle gives for the maximum value of the wind U at a given value of x :

$$U = vA(\frac{x}{h})^{-\frac{3}{4}} \tag{A4}$$

$$A^{'} = (\frac{C^{'}}{\gamma^3 h^2 v^2 (32\pi)^{\frac{1}{2}}\Lambda})^{\frac{1}{4}} \tag{A5}$$

$$C^{'} = -C = \frac{1}{2}\rho v_{vh}^2 C_D A h \tag{A6}$$

(A7)

with $A^{'}$ a constant, C_D the drag coefficient, h (m) the height of the vehicle, A (m^2) the cross-sectional area in the direction of motion, $C^{'}$ the flow couple on the vehicle, $\gamma = 0.4$ and $\Lambda = 4.13$ two coefficients estimated in Eskridge et al. 1979, ρ (kg m^{-3}) the density of the air. Refinements are possible by taking into account the other coordinates from the Eskridge et al. (1979) formula, the refined formula from Eskridge et al. (1982) or from Hider et al. (1997). Moreover, it could be possible to modelled with real formula the near-wake described by large-scale flow structures with high instabilities of the vehicle with other formula as the jet-plan turbulent flow power law $U \sim x^{-1/2}$ as defined in Youssef (2012).

https://doi.org/10.5194/egusphere-2025-2777
Preprint. Discussion started: 10 July 2025

Then, the average wind speed induced by the total traffic is modelled considering no overlap from the wind induced by each vehicle. The average wind speed is calculated along the vehicle and in the wake until the front of the next vehicle U_{traff}. To keep the formula consistent, it is assumed that the formula $U(x)$ is also valid in the near-wake of the vehicle (i.e x < 10h). However, a lower bound is determined (i.e x > l_{eff}) for continuity reason with the Couette flow U_l. Thus, the Couette flow is extended up to l_{eff} in the near-wake of a vehicle, then $U(x)$ is used further in the wake of the vehicle when $U(x) < U_l$. Thus, the length l_{eff} (m) calculated to keep the values of the wind speed within the limit $U(l_{eff}) < \frac{v}{2}$ is written as:

$$l_{eff} = \frac{h}{(2A)^{-\frac{4}{3}}} \tag{A8}$$

Then, an average wind speed induced by the entire traffic U_{traff} (m s^{-1}) is found by calculating the integral along the x-axis. The average wind speed induced by the vehicle fleet with U_{max} the wind induced behind the vehicle U_z the wind induced under the vehicle is expressed as:

$$U_{traff} = \frac{1}{(\frac{v}{\phi} + l + l_{eff})}\left(\int_{-l}^{l_{eff}} U_l\, dx + \int_{l_{eff}}^{v/\phi} U(x)\, dx\right) \tag{A9}$$

$$U_{traff} = \frac{1}{(\frac{v}{\phi} + l + l_{eff})}\left(\frac{v}{2}(l + l_{eff}) + 4Ah^{\frac{3}{4}} v\left(\left(\frac{v}{\phi}\right)^{\frac{1}{4}} - l_{eff}^{\frac{1}{4}}\right)\right) \tag{A10}$$

This formula has satisfactory boundary condition with $\lim_{v\to 0} U_{traff}(v) = 0$.

Finally with the heterogeneous driving conditions, we compute the average wind speed according to the underlying distribution of the vehicle speed. So for the average vehicle fleet speed $\overline{v}$ and the Monte-Carlo estimate $\overline{v^{\frac{1}{4}}}$ explained next section, we get:

$$U_{traff}(\overline{v}) \simeq \frac{1}{(\frac{\overline{v}}{\phi} + l + l_{eff})}\left(\frac{\overline{v}}{2}(l + l_{eff}) + 4Ah^{\frac{3}{4}}\overline{v}\left(\overline{v^{\frac{1}{4}}}(\phi)^{-\frac{1}{4}} - l_{eff}^{\frac{1}{4}}\right)\right) \tag{A11}$$

This formula is then adapated to the road lateral dimensions, mutliplied by the factor $\overline{w}/w_{rd}$ with $\overline{w}$ the mean vehicle width and w_{rd} the road width to get the average impact on the road dimensions.

In TEB, the sensible and latent heat fluxes between the road surface and the air layer are calculated at height z depending on the wind speed at the same level. Thus, the wind speed $U_{traff}(\overline{v})$ is modified by a vertical interpolation to height z by assuming a Monin–Obukhov log-wind profile under neutral conditions. First, the equality between Eq. (A11) and the log-wind profile at height $z_{traff} = \overline{h}/2$ is given as:

$$U_{traff}(\overline{v}) = \frac{u^*}{\kappa} ln\left(\frac{z_{traff}}{z_0}\right) \tag{A12}$$

The u^*/κ ratio is found with this previous formula and allow to caculate the wind induced by the traffic at height z with the same log-wind profile. Finnaly at height z the wind induced by the vehicle gives:

$$U_{traff}(z) = U_{traff}\frac{ln(\frac{z}{z_0})}{ln(\frac{z_{traff}}{z_0})} \tag{A13}$$

https://doi.org/10.5194/egusphere-2025-2777
Preprint. Discussion started: 10 July 2025

Appendix B: Estimation of the engine efficiency and fuel consumption of vehicles based on the WLTC dataset

B1 Method

To estimate the amount of energy lost from fuel combustion in a vehicle engine, one must consider the driver behaviour and the engine response. The WLTC dataset and an automobile fleet characteristics database are exploited. Four passenger car subcycles are considered, indexed by $s = \{1, 2, 3, 4\}$. They are characterised by low-speed, medium-speed, high-speed, and extra-high-speed regimes representative of different road speeds. First, the engine response is estimated in real-world scenario thanks to a databank of vehicle fuel consumption and characteristics and to the WLTC standard on the 4 subcycles. Four average vehicle engine efficiencies are estimated corresponding to the 4 subcycles. Second, thanks to the WLTC standard, estimates of average driver behaviours are calculated with monte-carlo estimators corresponding to the 4 subcycles. Finally, both vehicle engine efficiencies and estimates of average driver behaviours are extended for every possible vehicle fleet average speed $\overline{v}$ (m s^{-1}). A simple interpolation is carried out to get values between the 4 subcycles with multiple linear regression.

In France, the consumption of each commercially available car model is documented in a database managed by the Agence De l'Environnement et de la Maitrise de l'Energie (ADEME). This study uses a homogeneous database of vehicles sold between 2023 and 2024 as provided by Colas et al. (2025). Each vehicle has been driven through the WLTC cycle. The vehicle engine provides the force needed to counter the drag forces along the trajectory. The simple Newtonian law of motions models the different forces at stake with the standard equilibrium equation applied to the vehicle. Vehicles in the ADEME database include the latest vehicle models equipped with fuel saving technologies such as start and stop, and fuel injector cut-off.

The efficiency of the vehicle engine is strongly dependent on the engine engineering and differs from one engine to another. We could not access enough manufacturer data to accurately estimate the efficiency of all types of engines, so an indirect estimate of η_e was developed. The mechanical efficiency of the vehicle η_m is considered constant, since its variations for every driving condition are small compared to the variations of η_e.

The mean engine efficiency is computed. The start and stop technology turns off the vehicle engine when it is idle. The fuel injectors cut-off suppress the fuel consumption when the accelerator pedal is released. The traction force $F_{trac}(v_i)$ provided by a vehicle engine at each time step i can be broken down as:

$$\begin{cases} F_{trac}(v_i) & = F_r(v_i) + F_{aero}(v_i) + ma_i \qquad v_i \geq 0 \\ F_{trac}(v_i) & = 0 \qquad\qquad\qquad\quad v_i < 0 \end{cases} \tag{B1}$$

where F_r and F_{aero} are defined as in Eq. (5) and a_i (ms^{-2}) is the instantaneous acceleration. The parameters for the drag coefficient and the cross section area of the vehicle that are missing are inferred from Kukwein (Kühlwein, 2016). Other methods could be used to estimate these parameters when missing, such as the one in Komnos et al. (2024). For each vehicle along a WLTC cycle s, there exists a vehicle engine efficiency η_{se} that is a key variable that represents the energy lost by the

https://doi.org/10.5194/egusphere-2025-2777
Preprint. Discussion started: 10 July 2025

vehicles as defined by the system of equations Eq. (4). The vehicle engine efficiency can be computed as:

$$\eta_{se} = \frac{\frac{1}{n}\overline{v}_s \sum_{i=1}^{n} F_{trac}(v_i)}{\eta_m P_{fuel}} \tag{B2}$$

$$= \frac{1}{n\eta_m F_{fuel}}(m\sum_{i=1}^{n}\frac{dv_i}{dt} + \sum_{i=1}^{n} F_r(v_i) + \sum_{i=1}^{n} F_{aero}(v_i)) \tag{B3}$$

$$\tag{B4}$$

With m (kg) the car mass of a vehicle, η_m the mechanical efficiency of a vehicle set to 0.90 consistent with the estimates in Bera (Bera, 2019), n the number of measures along the subcycle s, $\overline{v}_s$ the average vehicle speed along the subcycle s, and P_{fuel} the total power generated by the fuel consumption of a vehicle written as:

$$P_{fuel} = \overline{v}_s \lambda_{fuel} \rho_{fuel} C \tag{B5}$$

With λ_{fuel} the heat of combustion in joule per kilogram, (43.8 10^6 J kg^{-1} for gasoline as in Pigeon et al. (Pigeon et al., 2007) and 41.0 10^6 J kg^{-1} for essence), ρ_{fuel} (kg m^{-3}) the fuel density given as 850 kg m^{-3} in this study and C (m^{3}m^{-1}) the fuel vehicle consumption.

This previous calculation is performed for each vehicle and then averaged to give an averaged engine efficiency of the automobile fleet given a specific subcycle $\overline{\eta_{se}}$. This value has two meanings. First, it represents the average vehicle engine efficiency of the total automobile fleet in the vehicle databank, but it also represents the average vehicle engine efficiency of the total automobile fleet at a given average speed $\overline{v}$ under real conditions. Indeed, we can assume that there is an underlying distribution of accelerations and speeds at each location. Each WLTC cycle has been built from a speed and acceleration data sample of the world's driving habits (Tutuianu et al., 2015). So there are two random variables X and Y in $\mathbb{R}$ for each WLTP subcycle of unknown probability density of speed $f_{X,s}$ and acceleration $f_{Y,s}$ such as $X \sim f_{X,s}(v)$ and $Y \sim f_{Y,s}(v)$ and v a parameter that is the average speed of the automobile fleet. Both random variables are considered independent within a WLTC subcycle. Speed and acceleration are also considered independent of the vehicle characteristics vector. Each WLTC subcycle is a Monte Carlo sampling of the underlying probability density of speed $f_{X,s}(U_k)$ and acceleration $f_{Y,s}(U_k)$ with U_k a suitable unknown Monte Carlo estimate. Then, the Monte Carlo samples are used to estimate the variables needed to estimate the traffic impact and to estimate the engine efficiencies $\overline{\eta_{se}}$ that depend on the driver behaviours.

Thus, $\overline{\eta_{se}}$ computed previously is an estimate of the average engine efficiency of the automobile fleet at a given average speed $\overline{v_s}$. The average speed $\overline{v_s}$ of the automobile fleet is computed from the Monte Carlo sampling as:

$$\overline{v_s} = \frac{1}{n}\sum_{k=1}^{n} X_{ks} \tag{B6}$$

https://doi.org/10.5194/egusphere-2025-2777
Preprint. Discussion started: 10 July 2025

Other estimates are needed to compute the average characeristics of the automobile fleet given the estimate of the expected value of X for a given subcycle s:

$$\overline{v_s^2} = \frac{1}{n}\sum_{k=1}^{n} X_{ks}^2 \tag{B7}$$

$$\overline{v_s^{\frac{1}{4}}} = \frac{1}{n}\sum_{k=1}^{n} X_{ks}^{\frac{1}{4}} \tag{B8}$$

$$\overline{p_s} = \frac{1}{n}\sum_{k=1}^{n} \mathbb{1}(Y_{ks} \geq 0) \tag{B9}$$

$$\overline{a_s} = \frac{1}{\overline{p_s} n}\sum_{k=1}^{\overline{p_s} n} Y_{ks}\mathbb{1}(Y_{ks} \geq 0) \tag{B10}$$

With, $\overline{v_s^2}$ the average estimate for the squared speed, $\overline{v^{\frac{1}{4}}}$ the average estimate for the power $\frac{1}{4}$ of the speed, and $\overline{p_s}$ the fraction of the total automomobile fleet with a positive or null acceleration, $\overline{a_s}$ the average estimate of the positive acceleration. Indeed, the negative acceleration does not contribute to the total force generated by the engine from Eq. (B1).

These terms are then extended for any given average speed $\overline{v}$. Regression equations are learnt to estimate the behaviour of the automobile fleet given the average speed $\overline{v}$. Simple multiple linear regressions (MLRs) are performed and give the estimates $\overline{v^{1/4}}(\overline{v})$, $\overline{v^2}(\overline{v})$, $\overline{p}(\overline{v})$ and $\overline{\eta_e}(\overline{v})$ drawn in Fig. B1. The positive acceleration $\overline{a}_s$ is averaged as a single value $\overline{a}$ = 0.28 since no simple relationship with the average speed $\overline{v}$ can be found. To keep the consistency with the dynamic of a real vehicle, two thresholds are added to these estimates at really low speed and high speed. The following conditions are satisfied:

$$\overline{p}(\overline{v}) \leq 0.54 \tag{B11}$$

$$\overline{\eta}(\overline{v}) \geq 0.08 \tag{B12}$$

The estimates of these variables are consistent with the physics of a vehicle motion. It is then included in TEB to compute the heat from the rolling resistance Eq. (5) and heat released in the air Eq. (9). The modelled key engine efficiency variable is comparable to the engine efficiency observed in a single vehicle (Kargul et al., 2016).

https://doi.org/10.5194/egusphere-2025-2777
Preprint. Discussion started: 10 July 2025

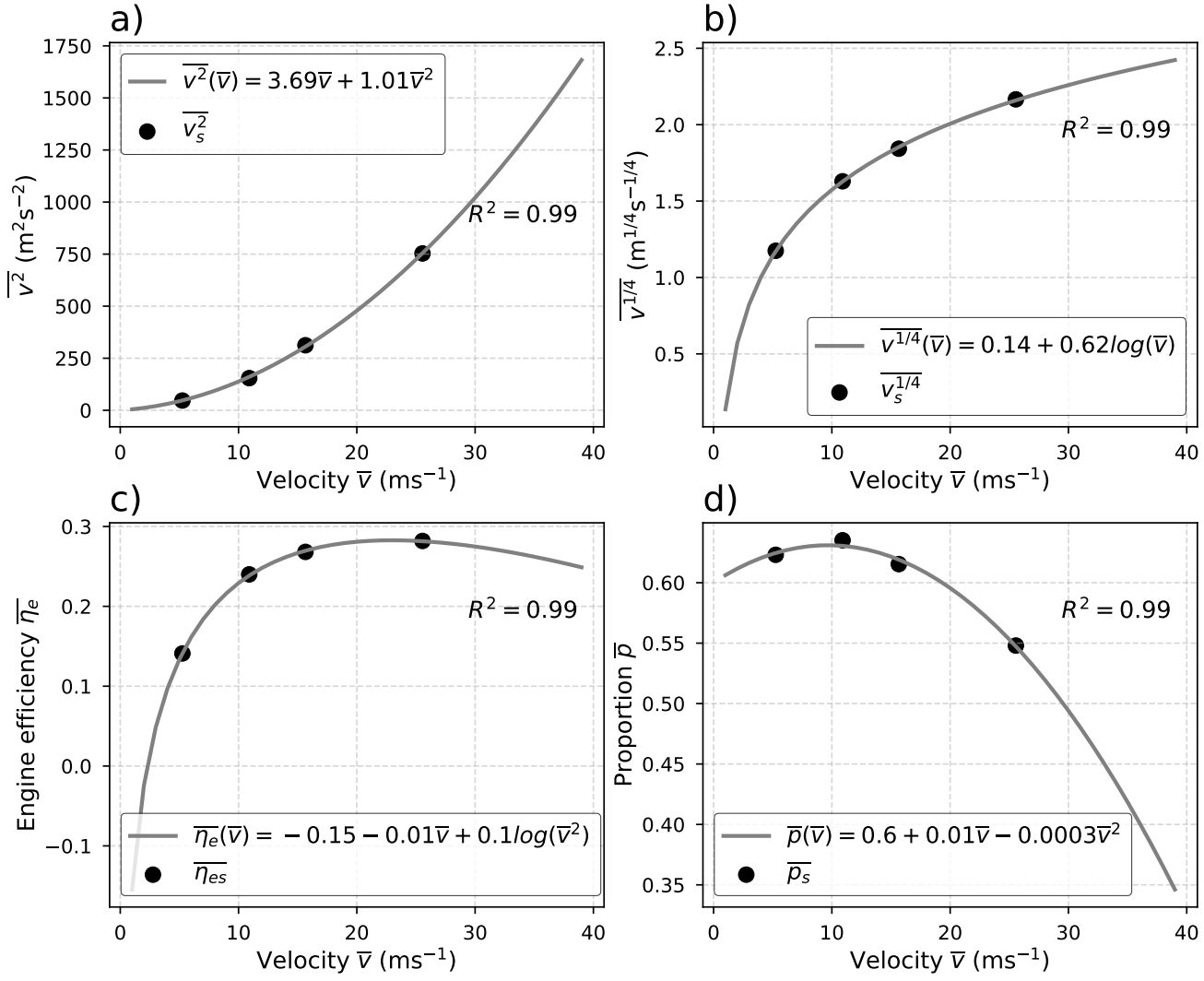

Figure B1. Regression equations from the multiple linear regressions (MLRs) of the parameters against the local estimate for each WLTC cycle with the average: (a) squared speed v_s^2, (b) speed to the power $1/4$, (c) engine efficiency, (d) acceleration proportion

B2 Evaluation

The method of estimating engine efficiency and other parameters related to fuel consumption is evaluated against the vehicle dataset. Since there is no direct measurement of the estimated variables, the fuel consumption of each vehicle from the WLTC subcycle is compared to the fuel consumption estimated as:

$$P_{fuel}(\overline{v}) = \frac{1}{\overline{\eta}(\overline{v})\eta_m}(F_r(\overline{v^2}(\overline{v})) + F_{aero}(\overline{v^2}(\overline{v})) + m\overline{a})\overline{p}(\overline{v})\overline{v} \tag{B13}$$

https://doi.org/10.5194/egusphere-2025-2777
Preprint. Discussion started: 10 July 2025

Inside this previous equation, every parameter needed to compute the heat released by a vehicle is used. This estimate can be used to retrieve the fuel consumption by averaging over a diversity of vehicles. This method allows to estimate the values of the parameters that have a significant impact on the heat lost by the vehicles.

595 The previous method is compared against a simple baseline without estimating the posterior parameters. This baseline is the average fuel consumption of the entire vehicle databank for each WTLC subcycle. Then it is tested against each vehicle fuel consumption in Fig. B2.

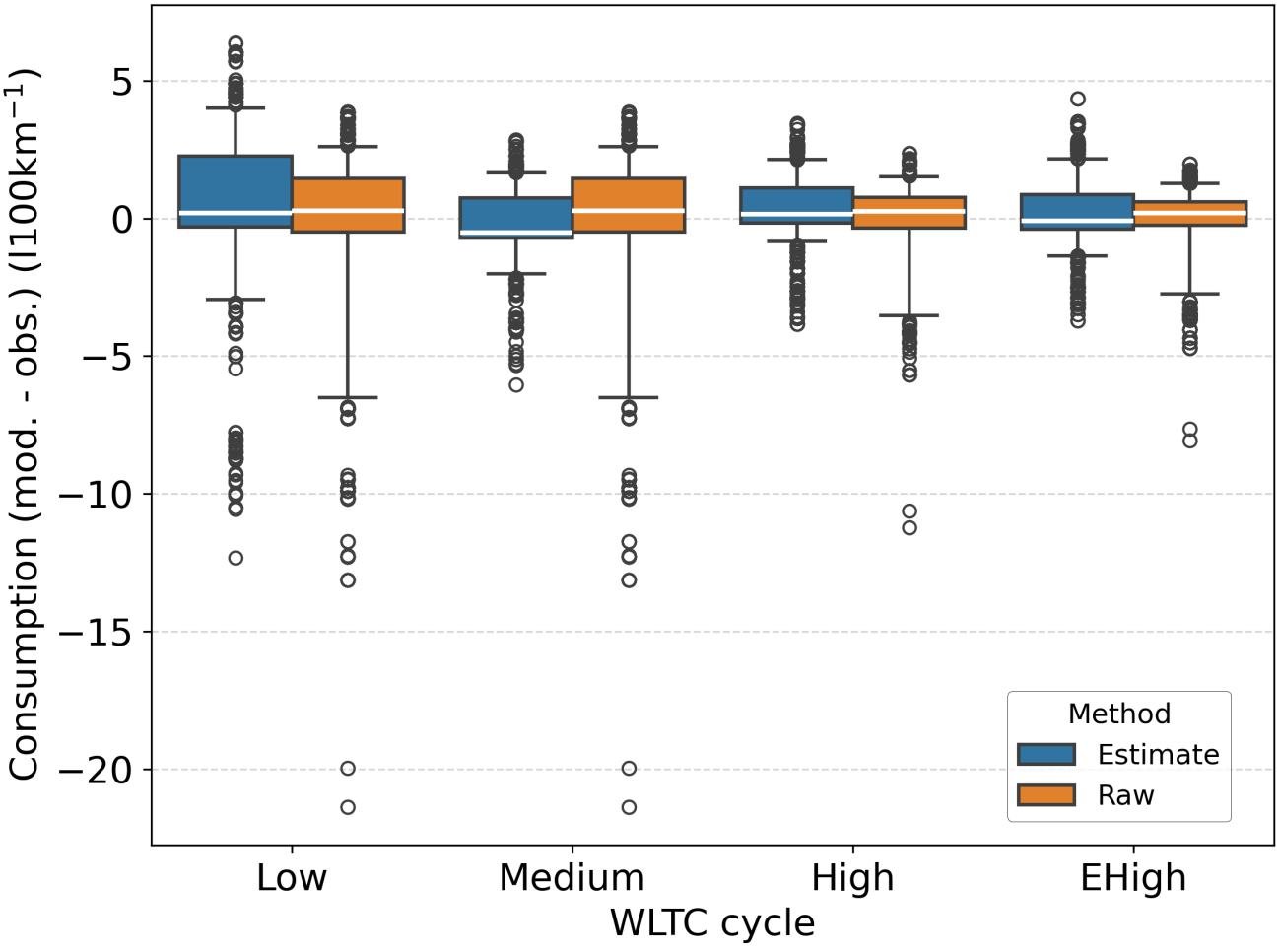

Figure B2. For each WLTC subcycle, boxplot of the difference between the fuel consumption modelled and the measurements for all the vehicles in the ADEME databank with the explicit method in blue and with a simple baseline which is the average fuel consumption for each WLTC subcycle in orange. The boxes extend from the first quartile (Q_1) to the third quartile (Q_3), with whiskers up to the farthest point lying within $1.5\times$ the interquartile range ($Q_3 - Q_1$).

https://doi.org/10.5194/egusphere-2025-2777
Preprint. Discussion started: 10 July 2025

Most fuel consumption estimates are within the range [-1, 2.5] (in litres per 100 km), as shown in Fig. B2. In this figure, outliers are composed of luxury and sports vehicles only, with a much higher fuel consumption. Since they are a very small part of the vehicle fleet, they are not representative of the behaviours of an average vehicle fleet. In addition, fuel consumption estimates are closer to the measured values as the WLTC subcycle increases. This can be explained by a lower fuel consumption variance between vehicle models as the mean speed increases. For instance, in the lower WLTC subcycles, the fuel consumption variance is larger. Thus, the estimates are less accurate. The baseline method performs better on average with lower variances in the low, high, and extra-high subcycles. However, the fuel consumption estimates are close enough to the real value to assume that the driver behaviour and engine efficiency estimates are satisfactory.

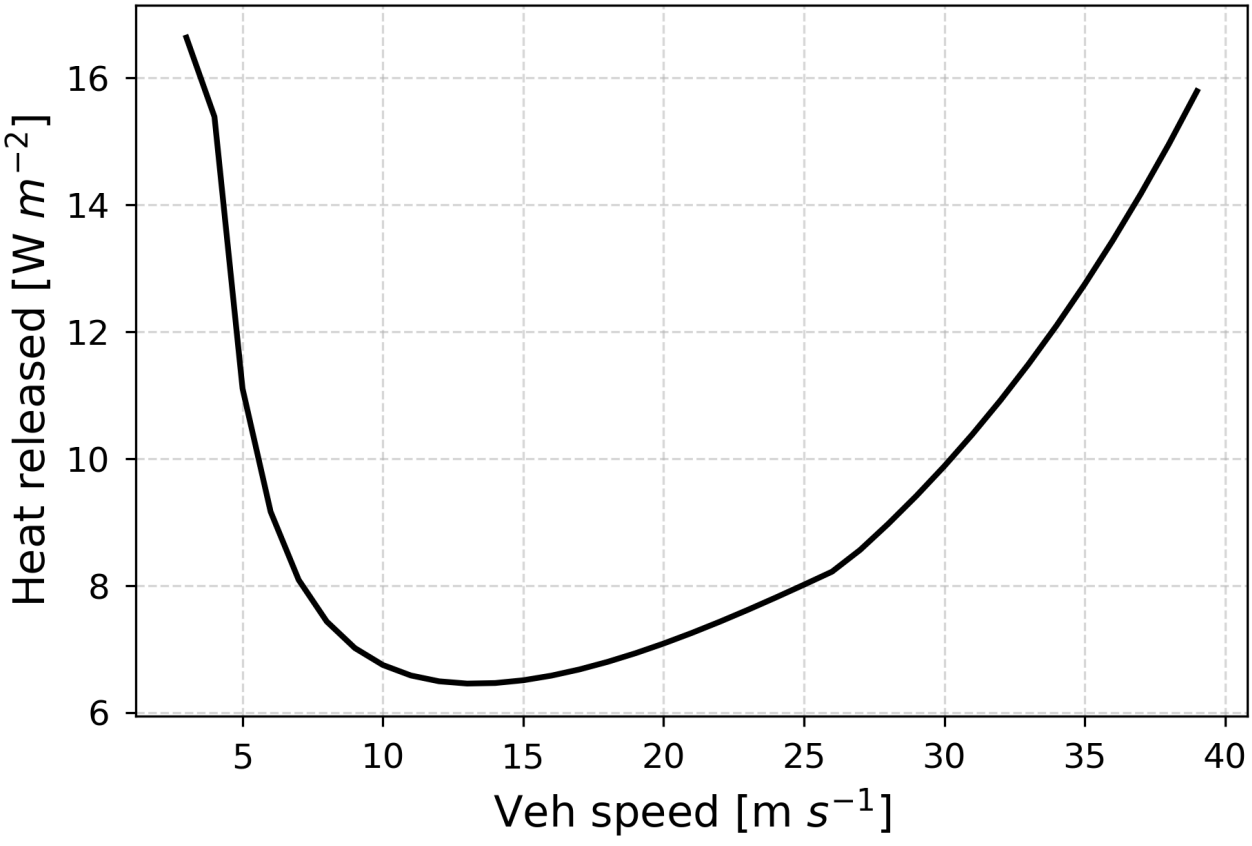

Figure B3. Power lost in a grid of 100 x 100m by the vehicles for a traffic intensity of 1400 veh h^{-1} and for common characteristics of vehicle for the Finland location

https://doi.org/10.5194/egusphere-2025-2777
Preprint. Discussion started: 10 July 2025

The total heat loss by the vehicle inefficiencies modelled in this study is comparable to the heat loss modelled in other studies. Pigeon et al. (2007) calulate 18.3 W m^{-2} released in the atmopshere for 1400 vehicles h^{-1} from the inventory approach in Toulouse city. In Fig. B3, the heat released by traffic is calculated considering the same traffic intensity (1400 vehicles h^{-1}) spread over the same area 100m x 100m. Depending on the average speed of road traffic in cities, this study simulates an average heat released from 16 W m^{-2} for 4 m s^{-1} to 6.3 W m^{-2} for 15 m s^{-1}. Despite, comparable values the heat released directly as sensible heat in the atmosphere is small compared to the values modelled previously in TEB as shown in Fig. B3. It can influence the analyses between this study and the studies based on inventories approach only.

Appendix C: Performances of the road surface temperatures simulated with the traffic impacts

TEB-CAR with the traffic impacts parameterised, and TEB are assessed with the road surface temperature (RST) observed in both directions. Common metrics are used to evaluate the performance of TEB-CAR and TEB, namely the mean squared error (MSE), the mean absolute error (MAE), the coefficient of determination (R^2) and the bias. A custom metrics is also used which is the mean time for a simulated variable to exceed a specific threshold in comparison with the observations named the average time threshold (ATT). Here, the ATT score calculate the average time the RST simulated reaches a value under 0.5 °C in comparison with the observations.

The traffic impacts parameterised in TEB-CAR lead to higher performance compared to the TEB simulation with lower RMSE, MAE, and significantly higher R^2 for the entire simulation, as shown in Table C1. In particular, TEB-CAR corrects the larger temperature differences between the simulations and observations, as shown by the strong decrease in MSE and the reduced interquartile range in the Fig. C1 for both locations. There is a larger simulation error from the TEB model for the Nupuri location than for Palojärvi, but after simulation correction from the traffic-induced effects, they reach equivalent performance. Knowing that the traffic intensity is higher at Nupuri than at Palojärvi, it could mean that TEB-CAR reasonably reproduces the traffic-induced effect on the RST. The variance is reduced by about the same amount between the two locations, giving confidence in the quality of the modelling in two different scenarios with different traffic. Furthermore, the ATT score in Table C1 shows that TEB-CAR improves the accuracy to predict plausible dangerous conditions (RST < 0.5°C) by 1°C on average.

https://doi.org/10.5194/egusphere-2025-2777
Preprint. Discussion started: 10 July 2025

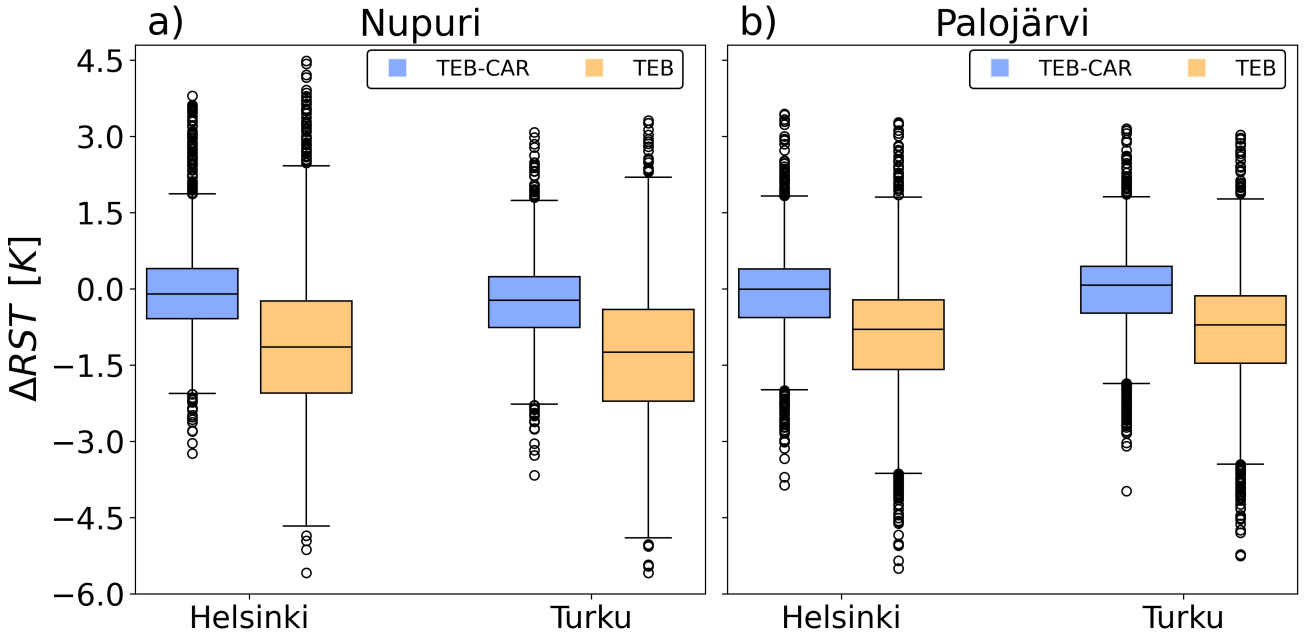

Figure C1. Boxplot of TEB and TEB-CAR simulations differences with the road surface temperature observations at Nupuri and Palojärvi location for the two directions, Helsinki and Tuku on joint Nupuri and Palojärvi period. The boxes extend from the first quartile (Q_1) to the third quartile (Q_3), with whiskers up to the farthest point lying within $1.5\times$ the interquartile range ($Q_3 - Q_1$).

Exp.	TEB Tur.	TEB-CARt Tur.	TEB Hel.	TEB-CARh Hel.
MSE	4.18	1.41	5.56	2.16
MAE	1.60	0.87	1.79	1.04
Biais	-0.41	-0.11	-0.10	0.25
R2	0.89	0.96	0.86	0.95
ATT (RST < 0.5 °C)	3.01	1.91	3.22	2.25

Table C1. Comparison of the model TEB with the road surface temperature in the Turku direction (Tur.) and Helsinki direction (Hel.) against TEB-CAR simulation for Turku direction (TEB-CARt) and for Helsinki direction (TEB-CARh) during the entire simulation.

https://doi.org/10.5194/egusphere-2025-2777
Preprint. Discussion started: 10 July 2025

Code and data availability. TEB is embedded in the software SURFEX available from the CNRM open-source website: https://opensource.umr-cnrm.fr (CNRM, 2025) under the CeCILL Free Software License Agreement v1.0. The TEB-CAR module corresponding to the changes made in SURFEX V9.0, the raw data to construct the experiments, the preprocess script to prepare the simulations, the simulation configurations and results, and the scripts to reproduce the figures are available on the Zenodo platform (https://doi.org/10.5281/zenodo.15640054, Colas 2025).

Author contributions. GC built the methodology and conceptualization, conducted the formal analysis, validation, visualization and wrote the paper. VM, FB and LB planned and supervised the project, participated to the methodology ,the validation and proofread the paper.

Competing interests. The authors declare that they have no conflict of interest

https://doi.org/10.5194/egusphere-2025-2777
Preprint. Discussion started: 10 July 2025

References

Ahmed, S.: An experimental study of the wake structures of typical automobile shapes, J. Wind Eng. Ind. Aerod., 9, 49–62, https://doi.org/10.1016/0167-6105(81)90077-5, 1981.

Amato, F., Favez, O., Pandolfi, M., Alastuey, A., Querol, X., Moukhtar, S., Bruge, B., Verlhac, S., Orza, J. A. G., Bonnaire, N., Le Priol, T., Petit, J. F., and Sciare, J.: Traffic induced particle resuspension in Paris: Emission factors and source contributions, Atmos. Environ., 129, 114–124, https://doi.org/10.1016/j.atmosenv.2016.01.022, 2016.

Baker, C.: Flow and dispersion in ground vehicle wakes, J. Fluid. Struct., 15, 1031–1060, https://doi.org/10.1006/jfls.2001.0385, 2001.

Bera, P.: A design method of selecting gear ratios in manual transmissions of modern passenger cars, Mech. Mach. Theory, 132, 133–153, https://doi.org/10.1016/j.mechmachtheory.2018.10.013, 2019.

Best, M. and Grimmond, C.: Investigation of the impact of anthropogenic heat flux within an urban land surface model and PILPS-urban, Theor Appl Climatol, 126, 51–60, https://doi.org/10.1007/s00704-015-1554-3, 2016.

Bohnenstengel, S. I., Hamilton, I., Davies, M., and Belcher, S. E.: Impact of anthropogenic heat emissions on London's temperatures, Quart. J. Roy. Meteorol. Soc., 140, 687–698, https://doi.org/10.1002/qj.2144, 2013.

Bueno, B., Pigeon, G., Norford, L. K., Zibouche, K., and Marchadier, C.: Development and evaluation of a building energy model integrated in the TEB scheme, Geosci. Model Dev., 5, 433–448, https://doi.org/10.5194/gmd-5-433-2012, publisher: Copernicus GmbH, 2012.

CNRM: CNRM Open Source, https:opensource.umr-cnrm.fr, 2025.

Colas, G.: Datasets, model and scripts for: Traffic impact modeling in SURFEX-TEB V9.0 model for improved road surface temperature prediction [code and data set], https://doi.org/10.5281/zenodo.15640054, 2025.

Colas, G., Masson, V., Bouttier, F., Bouilloud, L., Pavan, L., and Karsisto, V.: Improved winter conditions in SURFEX-TEB v9.0 with a multi-layer snow model and ice for road winter maintenance, EGUsphere [preprint], 2024, 1–31, https://doi.org/10.5194/egusphere-2024-1039, 2024.

Crevier, L.-P. and Delage, Y.: METRo: A and New Model and for Road-Condition and Forecasting in Canada, J. Appl. Meteorol., 40, 2026–2037, https://doi.org/https://doi.org/10.1175/1520-0450(2001)040<2026:MANMFR>2.0.CO;2, 2001.

de Munck, C., Pigeon, G., Masson, V., Meunier, F., Bousquet, P., Tréméac, B., Merchat, M., Poeuf, P., and Marchadier, C.: How much can air conditioning increase air temperatures for a city like Paris, France?, Int. J. Climatol., 33, 210–227, https://doi.org/10.1002/joc.3415, 2013.

De Ridder, K., Lauwaet, D., and Maiheu, B.: UrbClim – A fast urban boundary layer climate model, Urban Clim., 12, 21–48, https://doi.org/https://doi.org/10.1016/j.uclim.2015.01.001, 2015.

Denby, B. R., Sundvor, I., Johansson, C., Pirjola, L., Ketzel, M., Norman, M., Kupiainen, K., Gustafsson, M., Blomqvist, G., Kauhaniemi, M., and Omstedt, G.: A coupled road dust and surface moisture model to predict non-exhaust road traffic induced particle emissions (NOR-TRIP). Part 2: Surface moisture and salt impact modelling, Atmos. Environ., 81, 485–503, https://doi.org/10.1016/j.atmosenv.2013.09.003, 2013.

EEA: Sustainability of Europe's mobility systems, Tech. rep., European environmental agency, https://doi.org/10.2800/8560026, 2024.

Eskridge, R. and Rao, T.: Measurement and predicition of traffic-induced turbulence and velocity fields near roadways, J. Appl. Meteorol. Clim., 22, 1431–1443, https://doi.org/10.1175/1520-0450(1983)022<1431:MAPOTI>2.0.CO;2, 1983.

Eskridge, R. E. and Hunt, J. C. R.: Highway modelling. Part I: prediction of velocity and turbulence fields in the wake of vehicles, J. Appl. Meteorol. Clim., 18, 387–400, https://doi.org/10.1175/1520-0450(1979)018<0387:HMPIPO>2.0.CO;2, 1979.

https://doi.org/10.5194/egusphere-2025-2777
Preprint. Discussion started: 10 July 2025

Eskridge, R. E. and Thompson, R. S.: Experimental and theoretical study of the wake of a block-shaped vehicle in a shear-free boundary flow, Atmos. Environ. (1967), 16, 2821–2836, https://doi.org/https://doi.org/10.1016/0004-6981(82)90033-6, 1982.

Eurostat: Passenger cars, by type of motor energy, https://doi.org/10.2908/ROAD_EQS_CARPDA, 2023.

Farroni, F., Giordano, D., Russo, M., and Timpone, F.: TRT: thermo racing tyre a physical model to predict the tyre temperature distribution, Meccanica, 49, 707—-723, https://doi.org/10.1007/s11012-013-9821-9, 2014.

Flanner, M. G.: Integrating anthropogenic heat flux with global climate models, Geophys. Res. Lett., 36, L02 801, https://doi.org/https://doi.org/10.1029/2008GL036465, 2009.

Fujimoto, A., Watanabe, H., and Fukuhara, T.: Effects of vehicle heat on road surface temperature of dry condition, in: SIRWEC, Prague, Czech Republic, 2008.

Hargreaves, D. and Baker, C.: Gaussian puff model of an urban street canyon, J. Wind Eng. Ind. Aerod., 69-71, 927–939, https://doi.org/10.1016/S0167-6105(97)00218-3, 1997.

Harrison, R., McGoldrick, B., and Williams, C.: Artificial heat release from greater London, 1971–1976, Atmos. Environ. (1967), 18, 2291–2304, https://doi.org/https://doi.org/10.1016/0004-6981(84)90001-5, 1984.

Hider, Z., Hibberd, S., and Baker, C.: Modelling particulate dispersion in the wake of a vehicle, J. Wind Eng. Ind. Aerod., 67-68, 733–744, https://doi.org/10.1016/S0167-6105(97)00114-1, 1997.

Huber, P. J.: Robust Regression: Asymptotics, Conjectures and Monte Carlo, Ann. Statist., 1, 799 – 821, https://doi.org/10.1214/aos/1176342503, 1973.

Iamarino, M., Beevers, S., and Grimmond, C. S. B.: High-resolution (space, time) anthropogenic heat emissions: London 1970–2025, Int. J. Climatol., 32, 1754–1767, https://doi.org/10.1002/joc.2390, 2011.

ICCT: European vehicle market statistics, Tech. rep., International Council on Clean Transportation (ICCT), https://theicct.org/wp-content/uploads/2024/01/Pocketbook_202324_Web.pdf, 2023.

IPCC: Summary for Policymakers, p. In Press, Cambridge University Press, Cambridge, UK, in Press, 2022.

Jazar, R. N.: Vehicle dynamics: theory and applications, Springer, New York, NY, corrected at 3. printing edn., 2009.

Jin, L., Schubert, S., Fenner, D., Meier, F., and Schneider, C.: Integration of a Building Energy Model in an Urban Climate Model and its Application, Boundary Layer Meteorol., 178, 249—281, https://doi.org/10.1007/s10546-020-00569-y, 2021.

Johnson, T. and Joshi, A.: Review of vehicle engine efficiency and emissions, Tech. rep., SAE International, https://doi.org/10.4271/2018-01-0329, 2018.

Kargul, J., Moskalik, A., Barba, D., Newman, K., and Dekraker, P.: Estimating GHG reduction from combinations of current best-available and future powertrain and vehicle technologies for a midsized car using EPA's ALPHA model, SAE Technical Paper 2016-01-0910, SAE International, Warrendale, PA, https://doi.org/10.4271/2016-01-0910, iSSN: 0148-7191, 2688-3627, 2016.

Kargul, J., Moskalik, A., Barba, D., and Butters, K.: Validation of hybrid and electric vehicle models for ALPHA v3.0, SAE Technical Paper 2025-01-8521, SAE International, Warrendale, PA, https://doi.org/10.4271/2025-01-8521, iSSN: 0148-7191, 2688-3627, 2025.

Karsisto, V. E.: RoadSurf 1.1: open-source road weather model library, Geosci. Model Dev., 17, 4837–4853, https://doi.org/10.5194/gmd-17-4837-2024, 2024.

Kelly, D. P. and Sharp, R. S.: Time-optimal control of the race car: influence of a thermodynamic tyre model, Vehicle Syst. Dyn., 50, 641–662, https://doi.org/10.1080/00423114.2011.622406, 2012.

https://doi.org/10.5194/egusphere-2025-2777
Preprint. Discussion started: 10 July 2025

Khalifa, A., Marchetti, M., Bouilloud, L., Martin, E., Bues, M., and Chancibaut, K.: Accounting for anthropic energy flux of traffic in winter urban road surface temperature simulations with the TEB model, Geosci. Model Dev., 9, 547–565, https://doi.org/10.5194/gmd-9-547-2016, publisher: Copernicus GmbH, 2016.

Komnos, D., Broekaert, S., Zacharof, N., Ntziachristos, L., and Fontaras, G.: A method for quantifying the resistances of light and heavy-duty vehicles under in-use conditions, Energy Convers. Manage., 299, 117 810, https://doi.org/https://doi.org/10.1016/j.enconman.2023.117810, 2024.

Kühlwein, J.: Driving Resistances of light-duty vehicles in Europe: present situation, trends, and scenarios for 2025, , ICCT; International Council on Clean Transportation (2016), Tech. rep., International Council on Clean Transportation (ICCT), https://theicct.org/wp-content/uploads/2021/06/ICCT_LDV-Driving-Resistances-EU_121516.pdf, 2016.

Kłysik, K.: Spatial and seasonal distribution of anthropogenic heat emissions in Lodz, Poland, Atmos. Environ., 30, 3397–3404, https://doi.org/https://doi.org/10.1016/1352-2310(96)00043-X, 1996.

Lemonsu, A., Masson, V., Shashua-Bar, L., Erell, E., and Pearlmutter, D.: Inclusion of vegetation in the Town Energy Balance model for modelling urban green areas, Geosci. Model Dev., 5, 1377–1393, https://doi.org/10.5194/gmd-5-1377-2012, 2012.

Lemonsu, A., Viguié, V., Daniel, M., and Masson, V.: Vulnerability to heat waves: Impact of urban expansion scenarios on urban heat island and heat stress in Paris (France), Urban Clim., 14, 586–605, https://doi.org/10.1016/j.uclim.2015.10.007, 2015.

Lin, Y.-J. and Hwang, S.-J.: Temperature prediction of rolling tires by computer simulation, Math. Comput. Simulation, 67, 235–249, https://doi.org/10.1016/j.matcom.2004.07.002, 2004.

Lipson, M. J., Grimmond, S., Best, M., Abramowitz, G., Coutts, A., Tapper, N., Baik, J., Beyers, M., Blunn, L., Boussetta, S., Bou-Zeid, E., De Kauwe, M. G., De Munck, C., Demuzere, M., Fatichi, S., Fortuniak, K., Han, B., Hendry, M. A., Kikegawa, Y., Kondo, H., Lee, D., Lee, S., Lemonsu, A., Machado, T., Manoli, G., Martilli, A., Masson, V., McNorton, J., Meili, N., Meyer, D., Nice, K. A., Oleson, K. W., Park, S., Roth, M., Schoetter, R., Simón-Moral, A., Steeneveld, G., Sun, T., Takane, Y., Thatcher, M., Tsiringakis, A., Varentsov, M., Wang, C., Wang, Z., and Pitman, A. J.: Evaluation of 30 urban land surface models in the Urban-PLUMBER project: Phase 1 results, Quart. J. Roy. Meteorol. Soc., 150, 126–169, https://doi.org/10.1002/qj.4589, 2024.

Logan, J.: Modélisation des forces de contact entre le pneu d'un avion et la piste, Ph.D. thesis, Toulouse, ISAE, Toulouse, https://theses.fr/2012ESAE0019, 2012.

Masson, V. and Seity, Y.: Including Atmospheric Layers in Vegetation and Urban Offline Surface Schemes, J. Appl. Meteorol. Clim., 48, 1377 – 1397, https://doi.org/10.1175/2009JAMC1866.1, 2009.

Meng, C.: A numerical forecast model for road meteorology, Meteorol. Atmos. Phys., 130, 485–498, https://doi.org/10.1007/s00703-017-0527-8, 2018.

Newman, K., Kargul, J., and Barba, D.: Benchmarking and modeling of a conventional mid-size car using ALPHA, SAE Technical Paper 2015-01-1140, SAE International, Warrendale, PA, https://doi.org/10.4271/2015-01-1140, iSSN: 0148-7191, 2688-3627, 2015.

Newman, K. A. and Dekraker, P.: Modeling the effects of transmission gear count, ratio progression, and final drive ratio on fuel economy and performance using ALPHA, SAE Technical Paper 2016-01-1143, SAE International, Warrendale, PA, https://doi.org/10.4271/2016-01-1143, iSSN: 0148-7191, 2688-3627, 2016.

Newman, K. A., Doorlag, M., and Barba, D.: Modeling of a conventional mid-size car with CVT using ALPHA and comparable powertrain technologies, pp. 2016–01–1141, https://doi.org/10.4271/2016-01-1141, 2016.

Pacejka, H. B.: Modelling of Tyre Force and Moment Generation, in: Rolling Contact Phenomena, pp. 277–327, Springer Vienna, Vienna, https://doi.org/10.1007/978-3-7091-2782-7_5, 2000.

https://doi.org/10.5194/egusphere-2025-2777
Preprint. Discussion started: 10 July 2025

Pigeon, G., Legain, D., Durand, P., and Masson, V.: Anthropogenic heat release in an old European agglomeration (Toulouse, France), Int. J. Climatol., 27, 1969–1981, https://doi.org/10.1002/joc.1530, 2007.

Rao, K. S.: ROADWAY-2: A Model for Pollutant Dispersion near Highways, Water Air Soil Pollut., 2, 261–277, https://doi.org/10.1023/A:1021391519305, 2002.

Sailor, D. J. and Lu, L.: A top–down methodology for developing diurnal and seasonal anthropogenic heating profiles for urban areas, Atmos. Environ., 38, 2737–2748, https://doi.org/https://doi.org/10.1016/j.atmosenv.2004.01.034, 2004.

Sher, F., Chen, S., Raza, A., Rasheed, T., Razmkhah, O., Rashid, T., Rafi-ul Shan, P. M., and Erten, B.: Novel strategies to reduce engine emissions and improve energy efficiency in hybrid vehicles, Cleaner Engineering and Technology, 2, 100 074, https://doi.org/10.1016/j.clet.2021.100074, 2021.

Shourehdeli, S. A., Mirmohammadi, A., and Gholipour, H.: Machine learning-driven universal models for gasoline engine performance maps: Accuracy and generality evaluation, Thermal Science and Engineering Progress, 62, 103 593, https://doi.org/10.1016/j.tsep.2025.103593, 2025.

Stuhldreher, M., Kargul, J., Barba, D., McDonald, J., Bohac, S., Dekraker, P., and Moskalik, A.: Benchmarking a 2016 Honda Civic 1.5-Liter L15B7 Turbocharged Engine and Evaluating the Future Efficiency Potential of Turbocharged Engines, SAE International Journal of Engines, 11, 1273–1305, https://doi.org/10.4271/2018-01-0319, number: 2018-01-0319, 2018.

Tutuianu, M., Bonnel, P., Ciuffo, B., Haniu, T., Ichikawa, N., Marotta, A., Pavlovic, J., and Steven, H.: Development of the World-wide harmonized Light duty Test Cycle (WLTC) and a possible pathway for its introduction in the European legislation, Transportation Research Part D: Transport and Environment, 40, 61–75, https://doi.org/10.1016/j.trd.2015.07.011, 2015.

Varquez, A. C. G., Kiyomoto, S., Khanh, D. N., and Kanda, M.: Global 1-km present and future hourly anthropogenic heat flux, Sci. Data, 8, 64, https://doi.org/10.1038/s41597-021-00850-w, 2021.

Wahlin, J., Leisinger, S., and Klein-Paste, A.: The effect of sodium chloride solution on the hardness of compacted snow, Cold Reg. Sci. Technol., 102, 1–7, https://doi.org/10.1016/j.coldregions.2014.02.002, 2014.

Ward, H. C., Rotach, M. W., Gohm, A., Graus, M., Karl, T., Haid, M., Umek, L., and Muschinski, T.: Energy and mass exchange at an urban site in mountainous terrain – the Alpine city of Innsbruck, Atmos. Chem. Phys., 22, 6559–6593, https://doi.org/10.5194/acp-22-6559-2022, 2022.

Weiss, M., K.C., C., and Helmers, E.: Energy efficiency trade-offs in small to large electric vehicles, Environ Sci Eur, 32, 46, https://doi.org/10.1186/s12302-020-00307-8, 2020.

Youssef, J.: Étude expérimentale d'un jet plan turbulent se développant dans un flux uniforme en co-courant, Ph.D. thesis, ISAE-ENSMA Ecole Nationale Supérieure de Mécanique et d'Aérotechique, 2012.